## Supplementary Materials

### *Electrical status epilepticus rat model*

*Electrode implantation*

Rats were anesthetized with an intramuscular injection of ketamine (74 mg/kg; Alfasan, Woerden, the Netherlands) and xylazine (11 mg/kg; Bayer AG, Leverkusen, Germany), and placed in a stereotactic frame. In order to record hippocampal EEG, a pair of insulated stainless steel electrodes (70 μm wire diameter, tips 800 μm apart) was implanted into the left dentate gyrus under electrophysiological control as described previously (1). A pair of stimulation electrodes was implanted in the angular bundle. Two weeks after recovery from the operation, each rat was transferred to a recording cage (40x40x80 cm) and connected to a recording and stimulation system (NeuroData Digital Stimulator, Cygnus Technology Inc, USA) with a shielded multi-strand cable and electrical swivel (Air Precision, Le Plessis Robinson, France). A week after habituation to the new condition, rats underwent stimulation.

*Status epilepticus induction*

Rats underwent tetanic stimulation (50 Hz) of the hippocampus in the form of a succession of trains of pulses every 13 seconds. Each train was of 10 seconds duration and consisted of biphasic pulses (pulse duration 0.5 ms, maximal intensity 700 μA). Stimulation was stopped either after 90 minutes or when the rats displayed sustained forelimb clonus and salivation for several minutes, which usually occurred within one hour.

*EEG monitoring*

To determine seizure frequency, continuous EEG recordings (24 hours/day) were made in all rats. Hippocampal EEG signals were amplified (10x) by a high impedance headstage connected to an amplifier (20x; CyberAmp, Axon Instruments, Burlingame, CA, USA), band-pass filtered (1-60 Hz) and then digitized at 200 Hz (16 bit; Harmonie, Stellate Systems, Montreal, Canada).

All EEG recordings were visually screened and seizures were scored by trained human observers. Seizures are characterized by synchronized high-voltage amplitude oscillations and were scored when the amplitude increased more than 2-fold and lasted for at least 10 s.

***Rapid kindling rat model***

*Kindling stimulation*

EEG and stimulation electrodes were implanted as described in the preceding text. For EEG recording, the signals from the headstages were fed through commutators and a custom-designed filter and amplification unit (BR-20D Breakout Box, NPI electronic GmbH, Tamm, Germany). They were then sampled by a computer-controlled digitized card (NI USB-6255, National Instruments Netherlands, Woerden, the Netherlands) that also controlled the stimulation patterns in a synchronized way. EEG signals were amplified (10x within the headstage), band-pass filtered (0.1-1000 Hz), and then digitized at 2 kHz (16 bit; 30.5 μV/bit) using in-house data acquisition software running under MATLAB (MathWorks, Natick, MA, USA). EEG was recorded continuously during the experiment (24/7), starting 1 day before kindling (baseline). Stimulation was performed by the same NI USB-6255 multifunction I/O device, which was able to deliver biphasic, bipolar voltage stimulation pulses (max 20 V) at microsecond resolution to the selected stimulation channels of the headstage of each individual rat. Two ERB-24 USB-based 24-channel electromechanical relay interface devices (Measurement Computing Corporation, Norton, MA, USA), allowed us to multiplex the stimulations to the different rats in a time-efficient way. The perfect synchronization between stimulation and recording allowed adequate artifact suppression in the EEG recordings. In-house data acquisition software running under MATLAB (MathWorks, Natick, MA, USA) was used to evoke field potentials, to deliver the kindling stimulus, and to analyze EEG signals.

To determine the proper kindling stimulation intensity, for each animal the minimal intensity that saturated the field potential was determined as well as the stimulation intensity leading to a maximal field potential amplitude. Kindling stimulations were applied at 70% of the maximum stimulus intensity. For three subsequent days, rats were kindled (bipolar, biphasic 0.2 ms pulse (0.1 ms each), 50 Hz, for 10 sec, max amplitude 20 V) 12 times a day with 45-minute intervals. The first kindling stimulation on each day was given 1 hour after drug treatment. Animals were observed for 3 minutes after stimulation and behavioral seizures were scored using Racine's scale (2) by trained human observers. Rats were considered fully kindled if either i) five subsequent stage 5 seizures, ii) seven stage 5 seizures within one day or iii) a total of 10 stage 5 seizures were observed. After 11 days, a re-test was performed, in the absence of drug, during which rats received 7 stimulations in total.

*Preparation of rat brain tissue*

For RT-qPCR analysis, rats were decapitated at three different time points after SE, each corresponding to the phases of epileptogenesis: the acute phase (1 day post-SE, n=5), the latent phase (1 week post-SE, absence of electrographic seizures, n=6) and the chronic phase (3.5 months post-SE, recurrent spontaneous electrographic seizures are evident, n=5). In addition, 5 control rats were included. The brains were dissected and the parahippocampal cortex (PHC), which includes mainly the entorhinal cortex and parts of the perirhinal and posterior piriform cortex, was removed by incision at the ventro-caudal part underneath the rhinal fissure until approximately 5 mm posterior to bregma, as well as the hippocampus. The hippocampus was sliced into smaller parts (200–300 μm) and the DG and CA1 were cut out of the slices in 4˚C saline solution under a dissection microscope. All material was frozen on dry ice and stored at −80˚C until use.

For immunohistochemistry, rats were perfused at three different time points after SE, 1 day after SE (acute phase; n=5), 1 week after SE (latent phase; n=6) and 3.5 months after SE (chronic phase). During the chronic phase, we discriminated between rats that had progressive development of epilepsy (n=6) with on average 9 seizures/day in the week before they were sacrificed and rats that had non-progressive development of epilepsy with a low number of seizures (less than one seizure/week; non-progressive group, n=5). Furthermore, 5 control rats were included. Rats were deeply anesthetized with pentobarbital (Nembutal, 60 mg/kg) and perfused via the ascending aorta (300 mL 0.37% $Na^2S$ / 300 mL 4% paraformaldehyde in 0.1 M phosphate buffer, pH 7.4). After overnight post-fixation the brains were dissected and cryoprotected by overnight incubation (4°C) in 30% sucrose solution, buffered in 0.1 M phosphate buffer (pH 7.4). Thereafter, brains were frozen in isopentane (between -25°C and -30°C) and stored at -80°C until cutting.

***Intrahippocampal kainic acid mouse model***

*Implantations*

Littermate mice were randomly assigned in equal numbers to vehicle and IPR-179 groups. Before surgery, mice were anesthetized using isoflurane and placed in a stereotactic frame (SR-6M, Narishige Scientific Instrument, Japan). At the beginning of surgery, 0.5 mg carprofen (0.01 mL RYMDAL diluted with 1.5 mL saline) was given subcutaneously for pain relief. For intrahippocampal kainic acid injection, a 22 gauge cannula (diameter: 0.711/0.483 mm; length: 8.65 mm) was positioned above right hippocampal CA1 area (AP, -1.94; ML, +1.0; DV, 0.3 mm). For EEG recordings, an active skull electrode (mouse screw with 10 mm long wire and a pin adaptor attached, E363/96/1.6/Spc, Bilaney Consultants GmbH, Germany) was located close to cannula (AP, -1.94; ML, +2.0 mm); a reference electrode was implanted to the contralateral

hemisphere (AP, -3.50; ML, -3.5 mm); another 2 screws were implanted at approximately (AP, +2.5; ML, ±1.7 mm) as anchors. A 3D-printed headstage, designed to protect electrodes and hold an EEG transmitter and battery, was fixed together with cannula and screws by dental cement (Fig. S8). This design allows the EEG transmitter and battery to be held extracorporeally enabling battery exchange and consequently unlimited recording time. Immediately after surgery, the same dosage of carprofen/saline as above was administered subcutaneously. All animals were put under an infrared lamp and monitored until recovered from narcosis, then housed separately in an animal rack covered by a radio-frequency isolation net to create a Faraday cage and improve the quality of EEG recordings. Three days after surgery, once animals were habituated to the weight of the headstage and recovered from implantations, an EEG transmitter (A3028, Open Source Instruments, USA) was connected to the skull electrode. Three days later, we proceeded with the baseline recording of EEG and behavioral testing (for a scheme, see Fig. 6A). Two weeks after surgery, animals received intrahippocampal kainic acid injection.

*Intrahippocampal kainic acid injection*

Kainic acid monohydrate (K0250, Sigma Aldrich, Germany) was dissolved in Millipore distilled sterile water at concentration of 20 mM as stock solution and kept at -20°C. Thirty minutes before injection, the stock solution was diluted with Millipore water to 10 mM and loaded into a 10 µL Hamilton syringe with 35 gauge needle (NF35BV-2, World Precision Instruments, Sarasota, FL, USA). The Hamilton syringe was controlled by a MicroSyringe Pump Controller (Micro 4, World Precision Instruments, Sarasota, FL, USA). Animals with implantations were anesthetized and fixed to the stereotactic frame again. Through the cannula, 120 nL KA was administrated to the hippocampal CA1 area (AP, -1.94; ML, +1.0; DV, 1.3 mm) at a speed of 3 nL/s. After injection, animals were intensively monitored for behavioral and electrographic

seizures. Animals that showed stage 4 or 5 seizures according to Racine's scale (2) were recruited into the following experiments. The SE was terminated 1.5 hours after the first seizure with Lorazepam (6 mg/kg i.p.). The number of convulsions during the first hour after KA administration was recorded every 10 minutes to control that animals assigned to control and treatment groups showed seizures of equal severity. The analysis was performed by an experimenter blinded to the group assignments.

*EEG recording and analysis*

The EEG signals were recorded using a A3028 transmitter. This type of transmitter is composed of an analog input module, amplifier, filter, analog-to-digital converter module, transmitter antenna, magnetic switch module, and a holder for battery and replacement. The CR1225 lithium battery (Camelion Batterien GmbH, Berlin, Germany) was inserted into the battery holder (the typical operating life of the battery was 600 hours). After switching on the transmitter with a magnet, EEG signals were recorded at a sampling rate of 512 Hz, 100 times amplified, band-pass filtered (0.3-160 Hz), digitized (16 bit, roughly 0.4 μV/bit, this value is positively correlated with the battery voltage) and transmitted at central frequency in the range of 913-918 MHz at room temperature. The radio-frequency (RF) data from 10 transmitters were received by a 8-Loop-Antenna (A3015, Open Source Instruments, Watertown, MA, USA), which was connected to an Octal Data Receiver (A3027E, Open Source Instruments, Watertown, MA, USA) designed for reading out RF messages in the 902-928 MHz radio waves. Finally, the digital EEG signals were sent through ethernet to a recording computer using an LWDAQ driver (A2071E, Open Source Instruments, Watertown, MA, USA). EEG signals were continuously recorded in the freely moving mice using eight antennas of an Octal Data Receiver (A3027B, Open Source Instruments, Watertown, MA, USA) located in the IVC rack and the Neuroarchiver tool (ver.126, Open Source Instruments, Watertown, MA, USA) (3). The recordings were performed every other day

for up to 21 days after KA injection in the experiment with long-term IPR-179 treatment (to study antiseizure effects) whereas EEG signals were recorded continuously during the 1st and 2nd weeks and the 7th and 8th weeks after KA injection in the experiment with short-term IPR-179 treatment (to study antiepileptogenic effects).

The transmitter signals were reconstructed and recorded into archive files by data acquisition software Neuroarchiver 126 (Open Source Instruments, Watertown, MA, USA), glitches were excluded if they exceeded 5 × root mean square to avoid artefact introduced by transmitter collision. With the data processor ECP19v1, EEG signals were transformed into 7 metrics to describe the non-linear features of the signal (event power, coastline, intermittency, coherence, asymmetry, rhythm and spikiness; values are from 0 to 1, as defined at http://www.opensourceinstruments.com/Electronics/A3018/Seizure_Detection.html#Event%20Classification%20with%20ECP19). For automated epileptic event detection, a supervised machine learning strategy was applied. The Event Classifier for Neuroarchiver (OpenSource Instruments, Watertown, MA, USA) was used to establish a library of 1 second-long EEG epochs. Based on the amplitude and waveform of reconstructed EEG data and the results of discrete Fourier-transformation for each epoch, multiple events were manually added into the library and marked as basal, ictal and interictal events (http://www.opensourceinstruments.com/Electronics/A3018/Seizure_Detection.html) (4, 5). Figure 6D shows a typical projection of this library on a two-dimension plane. The X-axis represents the event power and the Y-axis represents the coastline. Each square represents a 1-second EEG epoch. The epochs used as templates clustered in 3 categories of events (light blue: baseline; black: interictal; red: ictal). Using this library, batch classification was applied to all EEG data using the 7 metrics computed by the ECP19v1 processor, as previously described (4, 5). In the experiment with short-term IPR-179 treatment we introduced an additional class of

events to exclude epochs containing noisy artefacts. The epileptiform period was defined as a period of time including ictal and interictal events. The criteria to define a seizure were: a period of time starting and ending with epileptiform epochs, lasting for at least 8 seconds, and interrupted by non-epileptiform activity less than 50% of the seizure period. The automatically detected electrophysiological seizures were confirmed by a trained observer. Application of the algorithm to data collected during a day before KA application, revealed a false-positive detection rate of approximately 0.1% or 0.2% in experiments with long- and short-term IPR-179 treatment, respectively.

*Behavioral tests*

*Open field test*

Animals were habituated for 3 days before the novel object recognition test was performed. During the first 2 days, animals were gently touched by an experimenter for 5 minutes, twice per day. On the third day, animals were exposed to an open field arena (50 x 50 x 30 cm) for 10 minutes. The behavioral video was recorded and analyzed by Anymaze 4.99 (Stoelting Co., Wood Dale, IL, USA). The distance traveled, time spent in the central zone and in the peripheral zone were measured.

*Novel object recognition test*

The novel object recognition test was performed prior to and 3 weeks after KA injection for the experiment with long-term IPR-179 treatment and 5 weeks after KA injection for the experiment with short-term IPR-179 treatment, using a standard protocol (6) that included two phases: a) a familiarization/encoding phase: mice were placed for 10 minutes in the arena, during which they could explore two identical objects positioned in the center of the arena; b) a test/retrieval phase: one familiar object and one novel object were placed in the center of the arena, and mice were

allowed to explore objects for 10 minutes (Fig. 7A). In the same trial, objects were counterbalanced, and between trials, different sets of objects were used. The interval between the encoding and retrieval phases was 24 hours. After video tracking by Anymaze, exploring time for familiar (TF) and novel (TN) objects as well as discrimination ratio ((TN-TF)/(TN+TF)) x100 were used to analyze animal's ability to recognize novel objects.

*Spatial navigation test in a labyrinth*

Mice in the experiment with long-term IPR-179 treatment were food-restricted for 2 days before the spatial navigation (labyrinth) test was performed. Animals were given about 1.5 g of test food (AIN-76A 10 mg tablets, TestDiet, St. Louis, MO, USA), which was offered as a reward in the labyrinth test. During this test, mice were given a maximum of 10 minutes to explore a labyrinth (60 x 60 x 12 cm; assembled from 3D-printed components as shown in Fig. 7D) and to find a reward dish (which had 10 tablets of test food in it) in a hidden corner. The animals' behavior was recorded and analyzed with Anymaze v4.99. Each recording was terminated 30 seconds after animals ate all food tablets. The latency to reward and the number of entries into non-reward corners were used to evaluate the spatial navigation skills.

*Novel object location test*

For the experiment with short-term IPR-179 treatment, the novel object location test was applied 9 weeks after KA injection. This test included two phases (7): a) a familiarization/encoding phase: mice were placed for 10 minutes in the arena, during which they could explore two identical objects positioned in the center of the arena; b) a test/retrieval phase: one object was moved to a different location at the arena, and mice were allowed to explore objects for 10 minutes. In the same trial, objects were counterbalanced, and between trials, different sets of objects were used. The interval between the encoding and retrieval phases was 24 hours. After video tracking by Anymaze v4.99, exploring time for familiar (TF) and novel (TN) locations as

well as discrimination ratio ((TN-TF)/(TN+TF)) x100 were used to analyze the animal's ability to recognize the novel object location.

***Real-time quantitative polymerase-chain reaction***

For RNA isolation, fresh human or rat brain material was homogenized in Qiazol Lysis Reagent (Qiagen Benelux, Venlo, the Netherlands). Total RNA was isolated using the miRNeasy Mini kit (Qiagen Benelux, Venlo, the Netherlands) according to the manufacturer's instructions. The concentration and purity of RNA were determined at 260/280 nm using a Nanodrop 2000 spectrophotometer (Thermo Fisher Scientific, Wilmington, DE, USA). To evaluate mRNA expression, 250-2000 ng of total RNA was reverse-transcribed into cDNA using oligo dT primers and run on a Roche Lightcycler 480 thermocycler (Roche Applied Science, Basel, Switzerland). The primers used for the study are listed in Table S6 and S7. Quantification of data was performed using LinRegPCR in which linear regression on the Log (fluorescence) per cycle number data is applied to determine the amplification efficiency per sample (8). The starting concentration of each specific product was divided by the geometric mean of the starting concentration of the reference genes elongation factor 1α (EF1α) and chromosome 1 open reading frame 43 (C1orf43) for human tissue and Glyceraldehyde-3-Phosphate Dehydrogenase (GAPDH) and Cyclophylin A for rat tissue, and this ratio was compared between groups.

***Immunohistochemistry***

Human brain tissue was fixed in 10% buffered formalin and embedded in paraffin. Paraffin-embedded tissue was sectioned at 5 μm, mounted on pre-coated glass slides (Star Frost, Waldemar Knittel, Braunschweig, Germany) and processed for immunohistochemical staining. Sections were deparaffinated in xylene, rinsed in ethanol (100%, 96%, 70%) and incubated for

20 minutes in 0.03% hydrogen peroxide diluted in methanol. Antigen retrieval was performed using a pressure cooker in 10 mM sodium citrate, pH 6.0 at 121°C for 10 minutes. Slides were washed with phosphate-buffered saline (PBS; pH 7.4) and incubated overnight with primary antibody (1:200 rabbit polyclonal anti-MMP2, ab37150, Abcam, Cambridge, UK; 1:100 rabbit monoclonal anti-MMP3, ab77962, Abcam, Cambridge, UK; 1:100 mouse monoclonal anti-MMP9, MAB13458, Millipore, Darmstadt, Germany; 1:500 mouse monoclonal anti-MMP14, MAB3317, Millipore, Darmstadt, Germany; 1:200 mouse monoclonal clone VT7 anti-TIMP1, Agilent, Santa Clara, CA, USA; 1:100 mouse monoclonal anti-TIMP2, MAB13446, Millipore, Darmstadt, Germany; 1:300 mouse monoclonal anti-TIMP3, MAB3318, Millipore, Darmstadt, Germany; 1:600 rabbit polyclonal anti-TIMP4, ab58425, Abcam, Cambridge, UK; 1:80,000, rabbit anti-albumin, DAKO, Glostrup, Denmark) in Normal Antibody Diluent (Immunologic, Duiven, the Netherlands) at 4°C. After washing in PBS, sections were stained with a polymer-based peroxidase immunohistochemistry detection kit (Brightvision plus kit, ImmunoLogic, Duiven, the Netherlands) according to the manufacturer's instructions. Staining was performed using Bright DAB substrate solution (ImmunoLogic, Duiven, the Netherlands). Sections were dehydrated in alcohol and xylene and coverslipped. The antibodies have been extensively tested for specificity. Previous studies have indicated their specificity with histology and blotting techniques for MMP2 (9-14), MMP3 (15, 16), MMP9 (17-19) and MMP14 (20-22).

Double-labeling of MMPs and TIMPs was performed with antibodies against neuronal nuclei (NeuN, 1:2,000 monoclonal mouse, MAB377, Merck, Amsterdam, the Netherlands), microtubule-associated protein 2 (MAP-2, 1:500 polyclonal rabbit, AB5622, Merck, Amsterdam, the Netherlands), glial fibrillary acidic protein (GFAP, 1:4,000 polyclonal rabbit, Z0334, DAKO, Glostrup, Denmark; or 1:4,000 monoclonal mouse, clone G-A-5, G-3893, Sigma, St. Louis, MO, USA), ionized calcium binding adaptor molecule 1 (IBA-1, 1:2,000 polyclonal rabbit, 019-

19741, WAKO, Richmond, VA, USA) or human leukocyte antigen DR/DP/DQ (clone CR3/43, 1:100 monoclonal mouse; M0775, DAKO, Glostrup, Denmark). After overnight incubation at 4°C and rinsing, sections were incubated with secondary antibodies, Alexa Fluor 488 donkey anti-mouse IgG (H+L) and Alexa Fluor 568 goat anti-rabbit IgG (H+L) (1:200, Invitrogen, Eugene, OR, USA) for two hours at room temperature and washed in PBS. Sections were coverslipped with Vectashield with DAPI (H-1200, Vector Laboratories Inc., Burlingame, CA, USA). Fluorescent microscopy was performed using a Leica Confocal Microscope TCS SP8-X (Leica, Son, the Netherlands).

Post-SE rat brains were cut using a sliding microtome and 40 μm horizontal sections were collected in tissue collecting solution (30% ethylene glycol and 25% glycerol in 0.05 M phosphate buffer) and stored at -20°C until immunohistochemistry was performed. Horizontal sections between 4100-4280 μm and 8600-8820 μm below the cortex surface of the contralateral brain part of control and post-SE rats were stained with different immunohistochemical markers. Free-floating sections were washed in 0.05 M PBS (pH 7.4) and incubated for 30 minutes in 0.3% hydrogen peroxide in PBS to inactivate endogenous peroxidase. Sections were then washed (2x10 minutes) in 0.05 M PBS, followed by washing (1x60 minutes) in PBS+0.5% Triton X-100+0.4% Bovine Serum Albumin (BSA). Sections were incubated overnight with primary antibodies (1:100 mouse monoclonal anti-MMP9, MAB13458, Millipore, Darmstadt, Germany) in PBS+0.1% Triton X-100+0.4% BSA at 4°C. After the incubation with the primary antibody, the sections were washed in PBS (3x10 minutes) and then incubated for 1.5 hours in biotinylated sheep anti-rabbit Ig (GE Healthcare, Diegem, Belgium), diluted 1:200 in PBS+0.1% Triton X-100. This was followed by 60-minute incubation in AB-mix (Vectastain ABC kit, Peroxidase Standard pk-4000, Vector Laboratories, Burlingame, CA, USA). After washing (3x10 minutes) in 0.05 M Tris-HCl, pH 7.9, the sections were stained with 10% DAB (Sigma-Aldrich,

Zwijndrecht, the Netherlands) and 0.015% $H_2O_2$ in Tris-HCl. The staining reaction was followed under the microscope and stopped by washing the sections in Tris-HCl. After mounting on Superfrost plus slides, the sections were air-dried, dehydrated in alcohol and xylene and coverslipped with Entellan (Merck, Darmstadt, Germany).

For the rapid kindling rat model, brains were collected directly after decapitation and the contralateral hemispheres were incubated in 4% paraformaldehyde for one week. Afterwards, tissue was embedded in paraffin and sectioned at 5 μm, mounted on pre-coated glass slides (Star Frost, Waldemar Knittel, Braunschweig, Germany). Immunohistochemistry followed the same protocol as used for human tissue discussed in the preceding text. Sections were incubated overnight at 4°C with NeuN (1:2,000 mouse monoclonal; MAB377, Merck, Amsterdam, the Netherlands). Staining was performed using 3,3'-diaminobenzidine substrate solution (1:10 in 0.05 M Tris-HCl, pH 7.6; ImmunoLogic, Duiven, the Netherlands). Sections were dehydrated in alcohol and xylene and coverslipped.

*Evaluation of immunohistochemistry*

MMP immunoreactivity was evaluated in neurons and cells with glial morphology within the human and rat dentate gyrus (DG) and CA1 by semi-quantitative analysis as described previously (23). The intensity of the staining was evaluated using a scale of 1-4 (1: no; 2: weak; 3: moderate; 4: strong staining). The score represents the predominant cell staining intensity found in each case. Additionally, the relative number of positive cells (0: no; 1: single to 10%; 2: 11-50%; 3: >50%) was also evaluated to give information about the relative number of positive cells. The immunoreactivity score (IRS) was calculated by multiplying the intensity score by the frequency score. Evaluation of neuron density in the dorsal and ventral hippocampi of rapid kindled rats was performed using Image-J with which NeuN-positive hilar cells were counted

and normalized to surface area of the respective hilus. The analyses were performed by an experimenter blinded to the group assignments.

*Western Blotting*

Ipsilateral temporal hippocampi of kindled rats were homogenized in 300 µL lysis buffer containing 50 mM Tris (pH 7.5) with 0.1% (v/v) Triton-X-100. Protein concentration was determined using the bicinchoninic acid method. For electrophoresis, equal amounts of proteins (50 µg/lane) were separated by sodium dodecylsulfate-polyacrylamide gel electrophoresis (SDS-PAGE, 10% acrylamide). Separated proteins were transferred to polyvinylidene fluoride (PVDF) paper by electroblotting for 1 hour and 30 minutes (Immobilon-P, Merck Millipore, Darmstadt, Germany). After blocking for 1 hour in TBS-T (20 mM Tris, 150 mM NaCl, 0.1% Tween, pH 7.5) / 5% non-fat dry milk, blots were incubated overnight at 4°C with the primary antibodies (Nectin-3, rabbit polyclonal, ab63931, Abcam, Cambridge, United Kingdom). After several washes in TBS-T, the membranes were incubated in TBS-T / 5% non-fat dry milk, containing goat anti-rabbit antibodies coupled to horse-radish peroxidase (1:2500; Dako, Glostrup, Denmark) for 1 hour. After washing in TBS-T, immunoreactivity was visualized using Enhanced Chemiluminescent (ECL) western blotting detection reagent (Thermo Fisher Scientific, Wilmington, DE, USA). Densitometry was used to quantify blots processed in parallel containing samples derived from the same experiment.

***Activity Assays***

*General conditions for activity assays*

The enzymatic reactions were performed in 96-well plates (Corning, Corning, NY, USA). Positive (no inhibitor) and negative (no enzyme) controls were included in each enzymatic assay.

All data were corrected by subtraction of their respective negative controls. All assays were conducted in triplicate at each point.

The percentage of inhibition for each titration point was calculated according to equation (I):

$$Inhibition\ activity\ (\%) = \left(1 - \frac{(a-b)}{(c-d)}\right)\ x\ 100 \qquad \text{(equation I)}$$

Where:

*a* corresponds to fluorescence intensity in the presence of substrate + IPR-179 + protease

*b* corresponds to the fluorescence intensity in the presence of substrate + IPR-179

*c* corresponds to the fluorescence intensity in the presence of substrate + protease

*d* corresponds to the fluorescence intensity in the presence of substrate

The $IC_{50}$ value was defined as the concentration of IPR-179 required to inhibit 50% of selected protease activity.

*MMP2 and MMP9*

In vitro enzymatic assays were performed as previously described (24). Briefly, the recombinant human MMP9 (Enzo Life Sciences Inc, Farmingdale, NY, USA) and recombinant human MMP2 (Merck, Darmstadt, Germany) were used in these assays at concentrations of 3.2 U/mL and 4.5 U/mL, respectively (100 µL total volume). For each assay, increasing concentrations of IPR-179 dissolved in dimethyl sulfoxide (DMSO, 2%) were used. Subsequently, DQ™-gelatin (Thermo Fisher, Waltham, MA, USA) was added (final concentration: 20 µg/mL). The plate was then placed immediately in a fluorescence plate reader, and fluorescence was measured every 5 min for 1 h at 25°C. The excitation and emission wavelengths were 483 nm and 525 nm, respectively.

*MMP1 and MMP7*

The recombinant human MMP1 (Enzo Life Sciences Inc, Farmingdale, NY, USA) and recombinant human MMP7 (Merck, Darmstadt, Germany) were used at concentrations of 93 U/mL and 0.74 U/mL, respectively (100 µL total volume). For each assay, increasing concentrations of IPR-179 dissolved in DMSO (2%) were used. Subsequently, Mca-PLGL-Dpa-AR-$NH_2$ fluorogenic substrate (R&D systems, Minneapolis, MN, USA) was added (final concentration: 10 µM). The plate was then immediately incubated at 25°C for 4 h, after which it was placed in a fluorescence plate reader (excitation 280 nm/emission 360 nm).

*MMP3*

The recombinant human MMP3 (Merck, Darmstadt, Germany) was used at a concentration of 217 U/mL (100 µL total volume). For each assay, increasing concentrations of IPR-179 dissolved in DMSO (2%) were used. After that, Mca-R-P-K-P-V-E-Nval-W-R-K(Dnp)–$NH_2$ fluorogenic substrate (R&D systems, Minneapolis, MN, USA) was added (final concentration: 10 µM). The plate was then immediately incubated at 25°C for 4 h, after which it was placed in a fluorescence plate reader (excitation 320 nm/emission 405 nm).

*MMP8*

In vitro enzymatic assays to determine the inhibitory profile against MMP8 proteases were performed using the SensoLyte® 490 assay kit (AnaSpec, Fermont, CA, USA) following the instructions of the provider. For each assay, increasing concentrations of IPR-179 dissolved in DMSO (2%). After a 15 preincubation period, EDANS/DabcylPlus™ peptide substrate was added (final concentration: 10 µM). The plate was then immediately incubated at 25°C for 2 h, after which it was placed in a fluorescence plate reader (excitation 340 nm/emission 490 nm).

*ADAM10 and ADAM17 (TACE)*

Activity assays for ADAM10 and ADAM17 were performed by Biology Corporation Inc (Malvern, USA). Briefly, the recombinant human ADAM10 (R&D systems, Minneapolis) and recombinant human ADAM17 (R&D systems, Minneapolis) were used at concentrations of 88 U/L and 39 U/L respectively. For each assay, increasing concentrations of IPR-179 dissolved in 2% DMSO were used. Subsequently, Mca-PLAQAV-Dpa-RSSSR-$NH_3$ peptide substrate was added (final concentration: 10 μM). The plate was then immediately incubated at 25°C for 2 h, after which it was placed in a fluorescence plate reader (excitation 340 nm/emission 405 nm).

*Prolyl oligopeptidase (POP)*

POP was obtained by expression in E. coli and affinity purification as previously described (25) and used at a concentration of 0.1 U/L during the assay (140 μL total volume). POP activity was measured following the method described by Toide et al. (26). The reactions were performed in 96-well microplates, thereby allowing the simultaneous monitoring of multiple reactions. For each assay, increasing concentrations of IPR-179 dissolved in 2% DMSO were used. After a preincubation of 15 min at 37°C, the Cbz-Gly-Pro-AMC substrate (Bachem, Bubendorf, Switzerland) was added to each well (final concentration: 200 μM). The 96-well plate was then immediately incubated at 37°C for 1 h, after which it was placed in a fluorescence plate reader (excitation 360 nm/emission 485 nm).

*Dipeptidyl peptidase-4 (DPP-IV)*

The ectodomain (residues 39-766) of DPPIV was obtained by expression in Sf9 insect cells using the Baculovirus technique and used at a concentration of 0.5 U/L during the assay (140 μL total volume). PDDIV activity was determined following the method previously described (27). For

each assay, increasing concentrations of IPR-179 dissolved in 2% DMSO were used. After a preincubation of 15 min at 37°C, the H-Gly-Pro-AMC substrate (Bachem Bubendorf, Switzerland) was added (final concentration: 50 μM). The plate was then immediately incubated at 37°C for 1 h, after which it was placed in a fluorescence plate reader (excitation 360 nm/emission 485 nm).

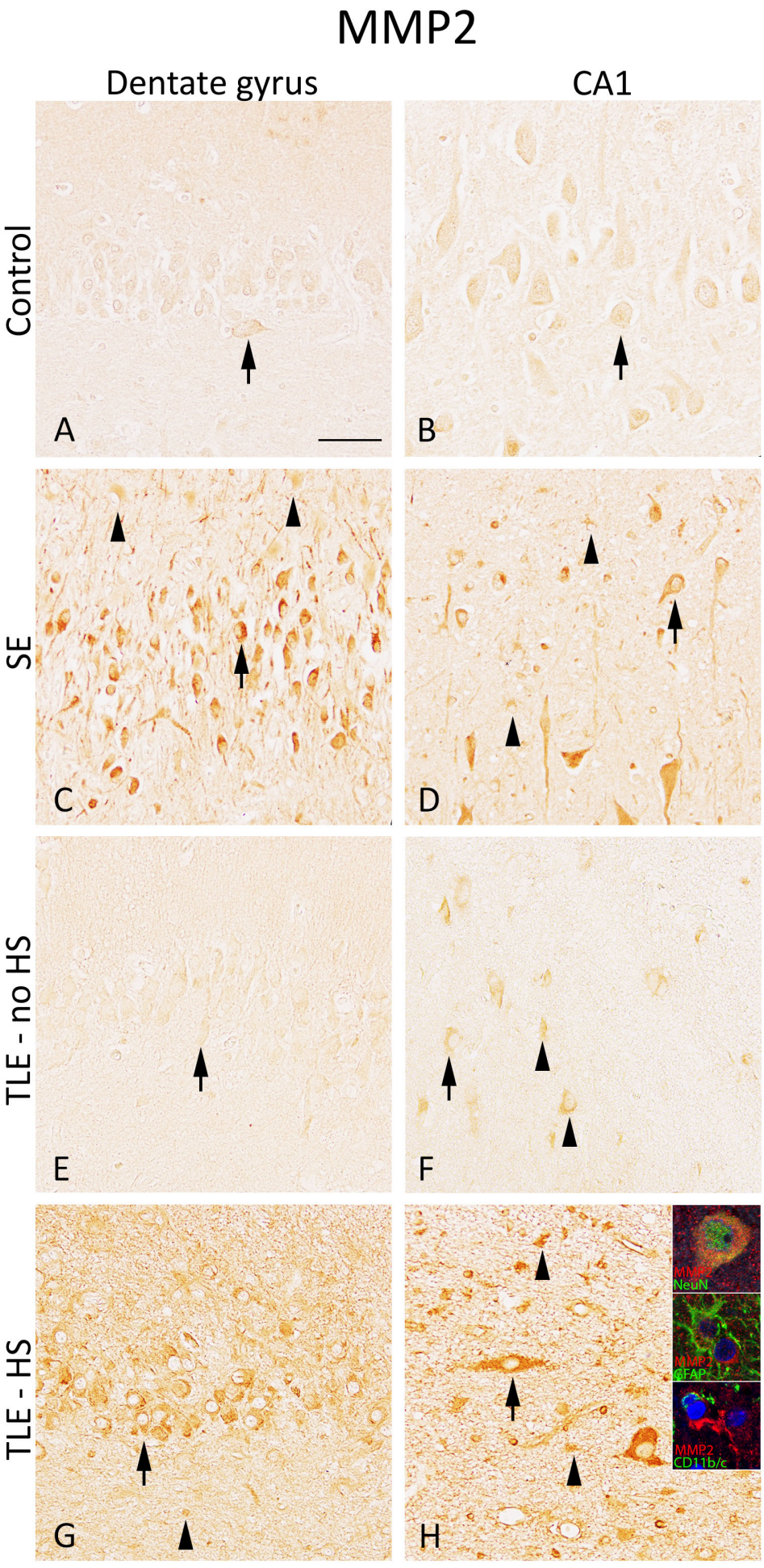


**Supplementary Figure 1. Expression of MMP2 in the dentate gyrus and CA1 of the human hippocampus.**

In controls, MMP2 was moderately expressed in neurons and no to weak expression was observed in glial cells (A, B). Patients who died after SE had higher MMP2 expression in both neurons and glial cells (C, D) as compared to controls. Patients with temporal lobe epilepsy (TLE) without hippocampal sclerosis (no-HS) had higher MMP2 expression in glial cells within CA1 compared to controls. Patients with TLE and hippocampal sclerosis (HS) had higher MMP2 expression in neurons and glia of the dentate gyrus, as well as in CA1 (E-H). Scale bar= 50 µm. Arrowheads indicate positive cells with glial morphology. Arrows indicate positive neurons. Insets depict double labeling of MMP2 in NeuN-positive cells (neurons) and GFAP-positive cells (astrocytes), but not in CR3/43-positive cells (microglia).

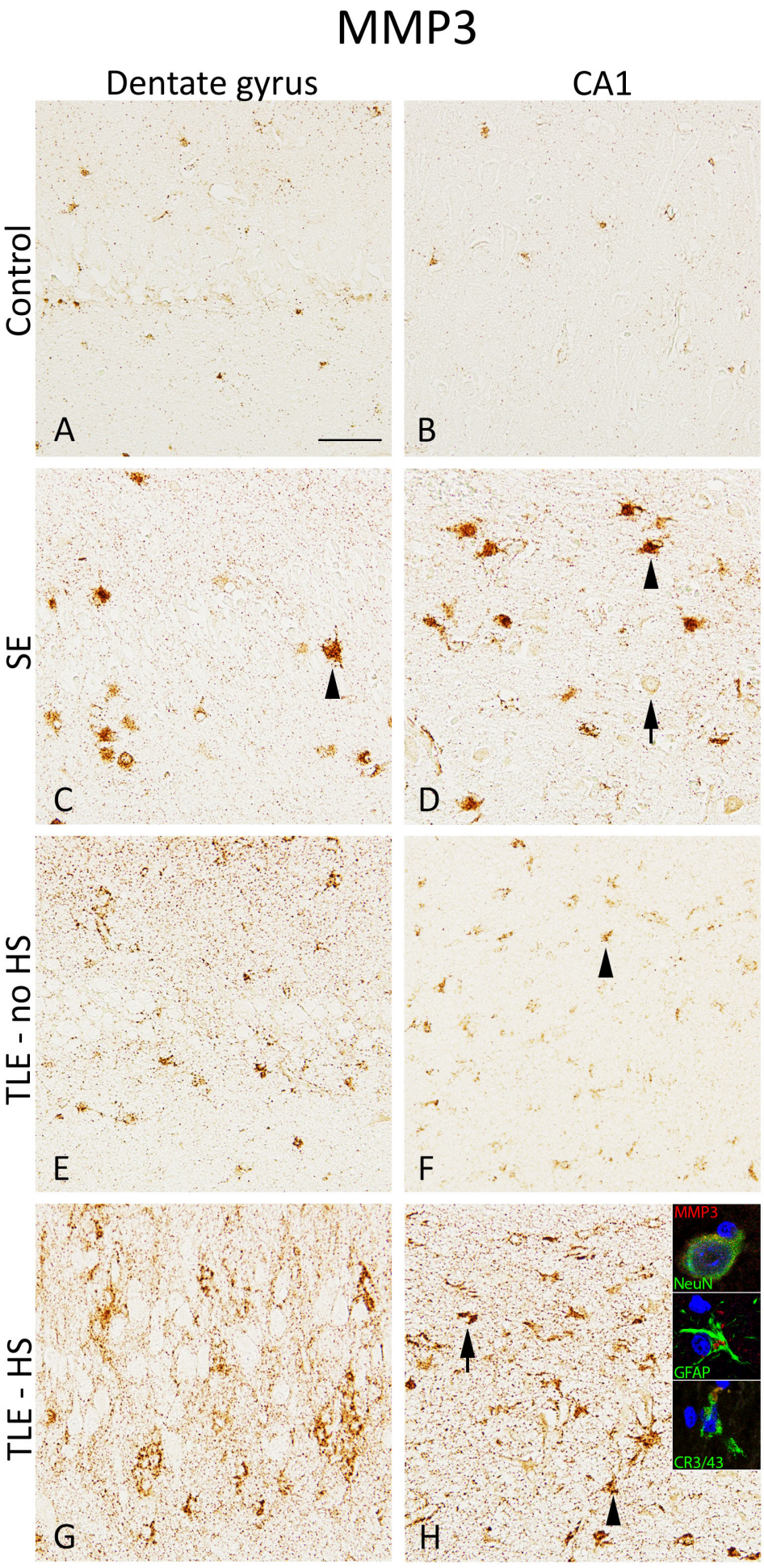


**Supplementary Figure 2. Expression of MMP3 in the dentate gyrus and CA1 of the human hippocampus.**

In controls, MMP3 was moderately expressed in glial cells, while no-low immunoreactivity was detected in neurons (A, B). In patients that died after status epilepticus (SE; C, D), as well as in patients with temporal lobe epilepsy (TLE) without hippocampal sclerosis (no-HS; E, F), MMP3 expression was increased in glial cells within the DG and CA1 and in CA1 pyramidal cells as compared to controls. In patients with TLE and HS (G, H) a similar pattern was observed, except in CA1, in which MMP3 expression was higher in CA1 (both in glia and in pyramidal cells) as compared to TLE - no HS. Scale bar= 50 µm. Arrowheads indicate positive cells with glial morphology. Arrows indicate positive neurons. Insets depict double labeling of MMP3 in NeuN-positive cells (neurons), GFAP-positive cells (astrocytes) and CR3/43-positive cells (microglia).

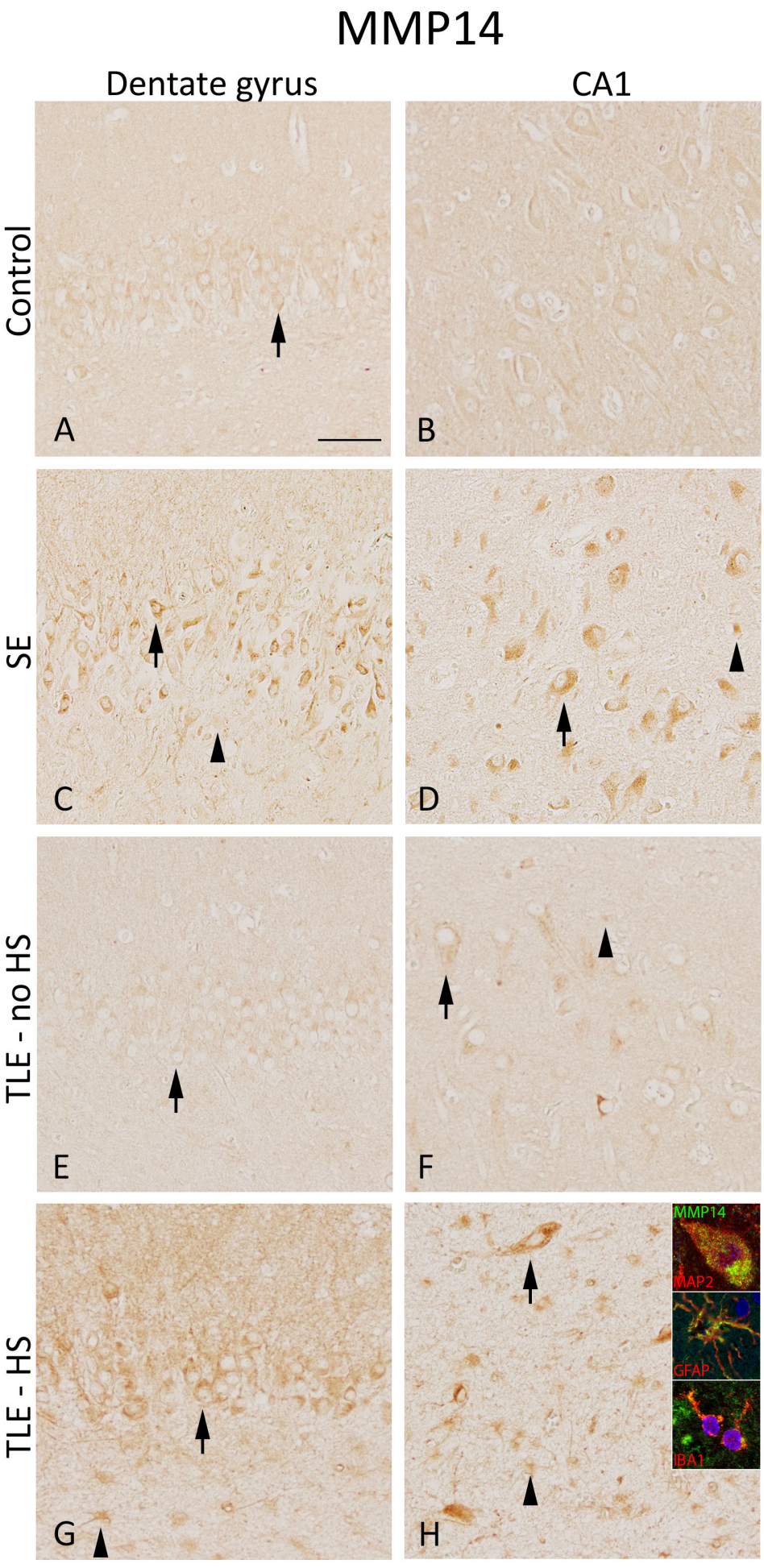


**Supplementary Figure 3. Expression of MMP14 in the dentate gyrus and CA1 of the human hippocampus.**

In controls, MMP14 was moderately expressed in neurons and weakly expressed in glial cells (A, B). Higher MMP14 expression was observed in both neurons and glia of the hippocampus from patients who died after status epilepticus (SE; C, D). In patients with temporal lobe epilepsy (TLE) without hippocampal sclerosis (no-HS; E, F), MMP14 expression was higher in glia within CA1 as compared to controls. MMP14 expression was higher in glia and neurons within CA1 in patients with TLE and HS (G, H). Scale bar= 50 µm. Arrowheads indicate positive cells with glial morphology. Arrows indicate positive neurons. Insets depict double labeling of MMP14 in MAP-2-positive cells (neurons) and GFAP-positive cells (astrocytes), but not in IBA-1-positive cells (microglia).

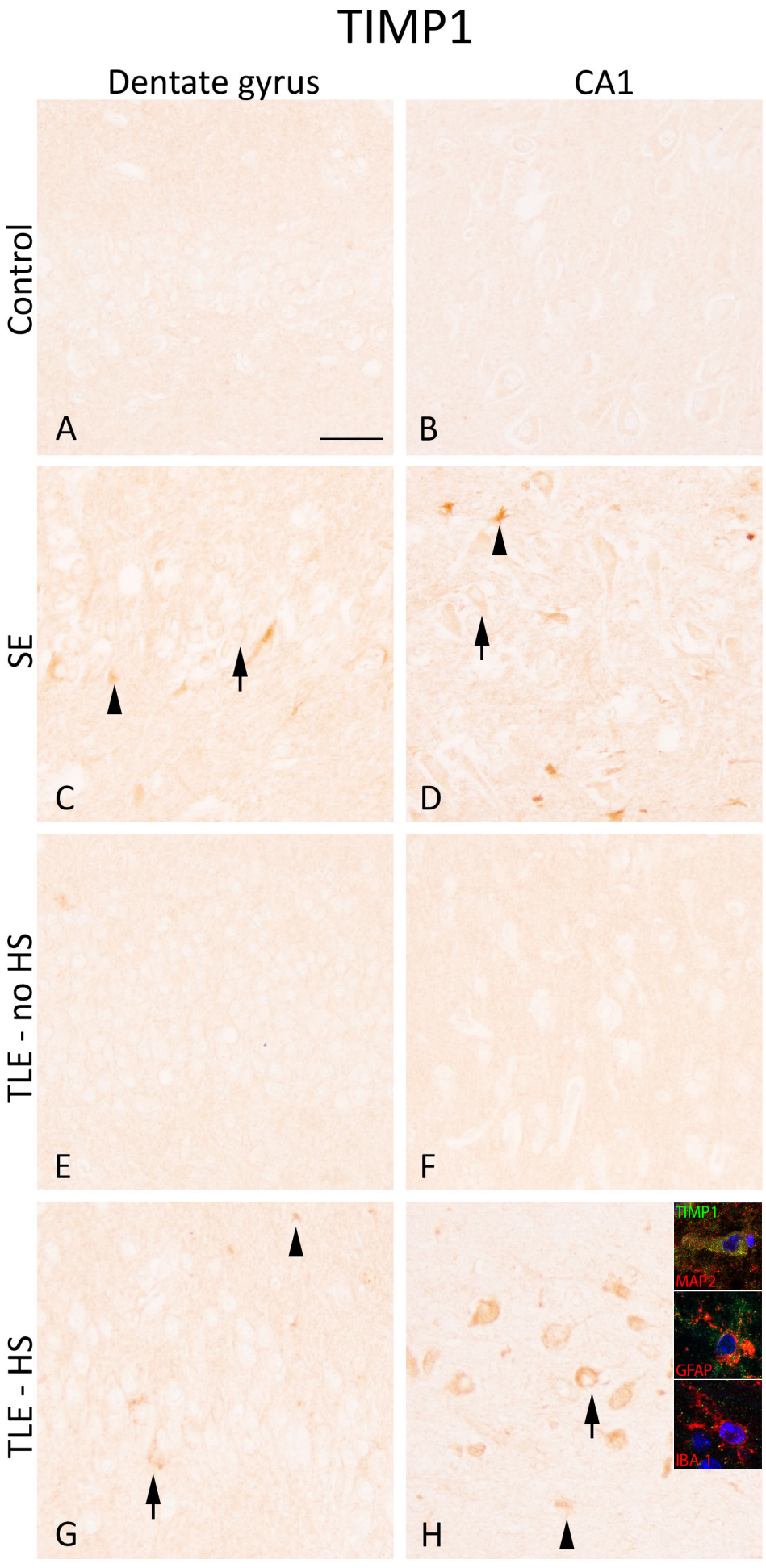


**Supplementary Figure 4. Expression of TIMP1 in the dentate gyrus and CA1 of the human hippocampus.**

In controls, TIMP1 protein expression is weak in both neurons and glial cells (A, B). Moderate expression was seen in neurons and glial cells of patients who died after a status epilepticus (SE), while expression was higher in glial cells compared to controls (C, D). In patients with temporal lobe epilepsy without hippocampal sclerosis (TLE - no HS), TIMP1 expression was weak in neurons and glial cells (E, F). In TLE - HS, TIMP1 expression was higher in CA1 neurons and in glial cells within the DG and CA1 (G, H). Scale bar= 50 µm. Arrowheads indicate positive cells with glial morphology. Arrows indicate positive neurons. Insets depict double labeling of TIMP1 with MAP-2-postive cells (neurons) and GFAP-positive cells (astrocytes), but not in IBA-1-positive cells (microglia).

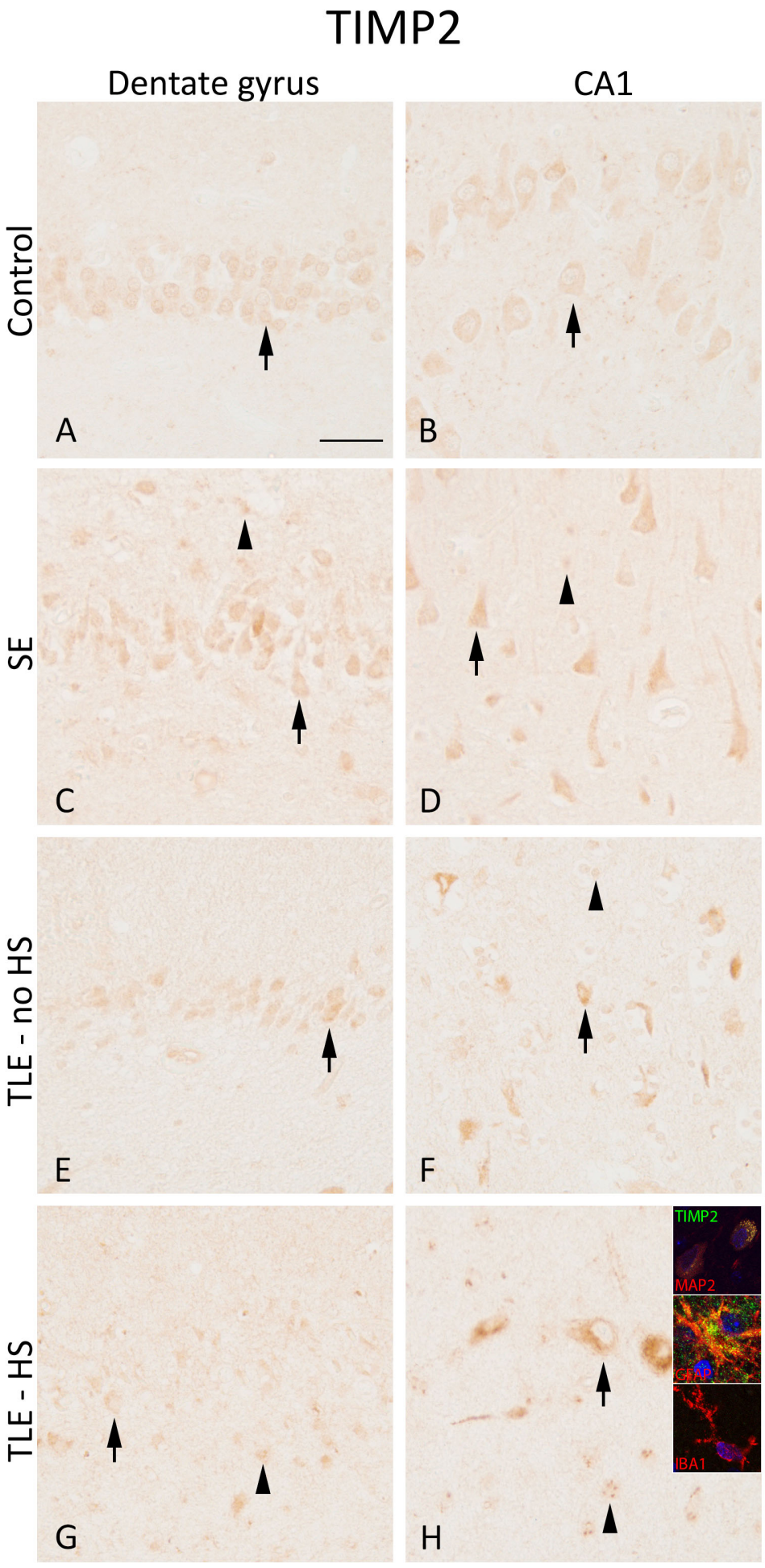


**Supplementary Figure 5. Expression of TIMP2 in the dentate gyrus and CA1 of the human hippocampus.**

In controls, TIMP2 was moderately expressed in neurons, while no to weak expression was observed in glial cells (A, B). Patients who died after status epilepticus (SE) showed higher expression in both neurons and glial cells compared to controls (C, D). Temporal lobe epilepsy patients without hippocampal sclerosis (TLE – no HS) had higher expression in DG neurons and glia within the CA1 as compared to controls (E, F). In TLE – HS patients, glial expression in DG and CA1, and neuronal expression in CA1 was increased compared to controls and TLE – no HS patients (G, H). Scale bar 50µm. Arrowheads indicate positive cells with glial morphology. Arrows indicate positive neurons. Insets depict double labeling of TIMP2 in MAP-2-positive cells (neurons) and GFAP-positive cells (astrocytes), but not in IBA-1-positive cells (microglia).

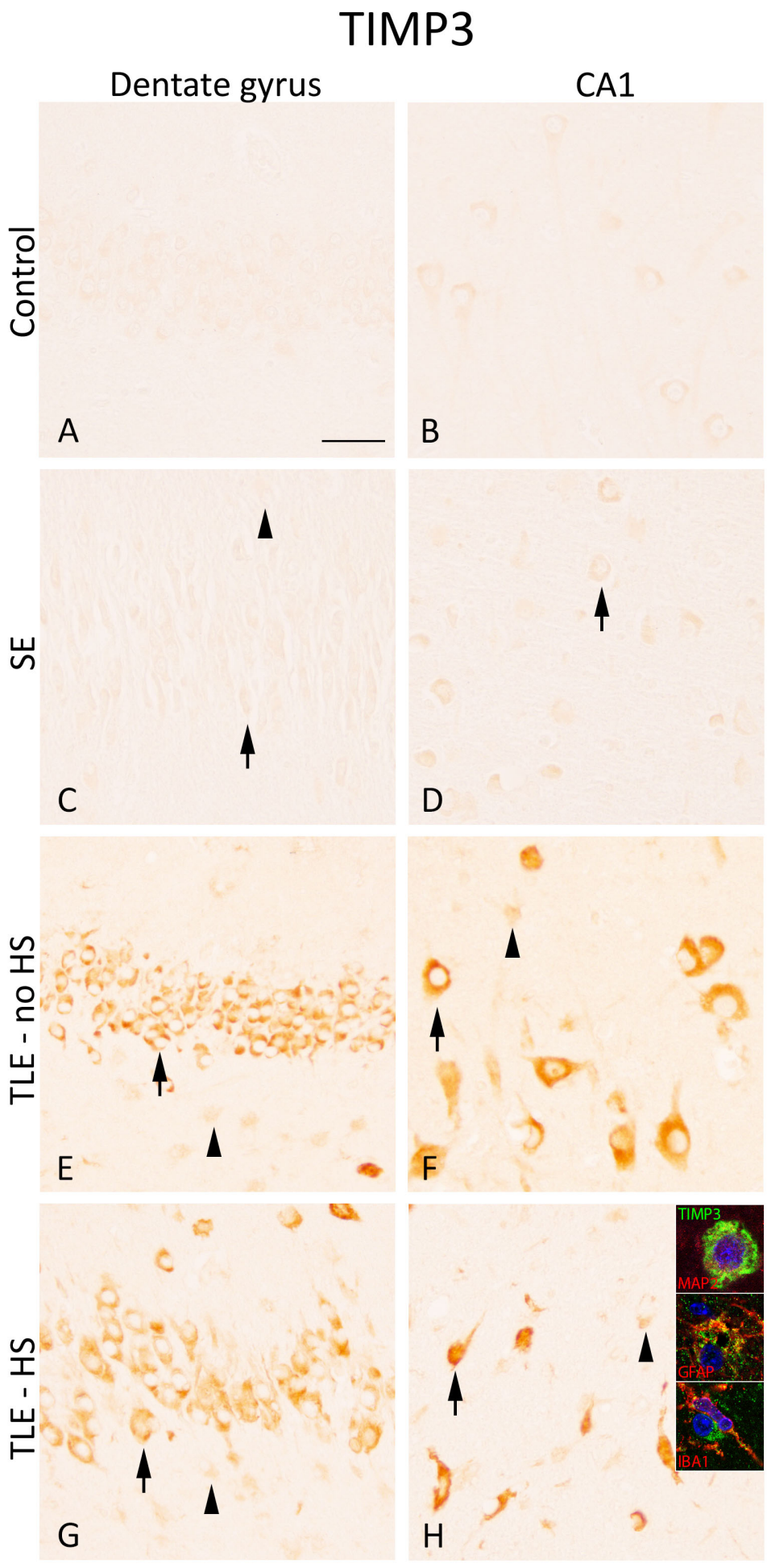


**Supplementary Figure 6. Expression of TIMP3 in the dentate gyrus and CA1 of the human hippocampus.**

In controls, TIMP3 is weakly to moderately expressed in neurons, while no expression was seen in glial cells (A, B). In patients who died after a status epilepticus (SE), weak to moderate TIMP3 expression was observed in neurons and higher expression was seen in glia of the dentate gyrus (C, D). In patients with temporal lobe epilepsy (TLE), TIMP3 expression was higher in both neurons and glia within the DG and CA1 (E-H) as compared to controls. HS, hippocampal sclerosis. Scale bar= 50 µm. Arrowheads indicate positive cells with glial morphology. Arrows indicate positive neurons. Insets depict double labeling of TIMP3 in MAP-2-positive cells (neurons), GFAP-positive cells (astrocytes) and IBA-1-positive cells (microglia).

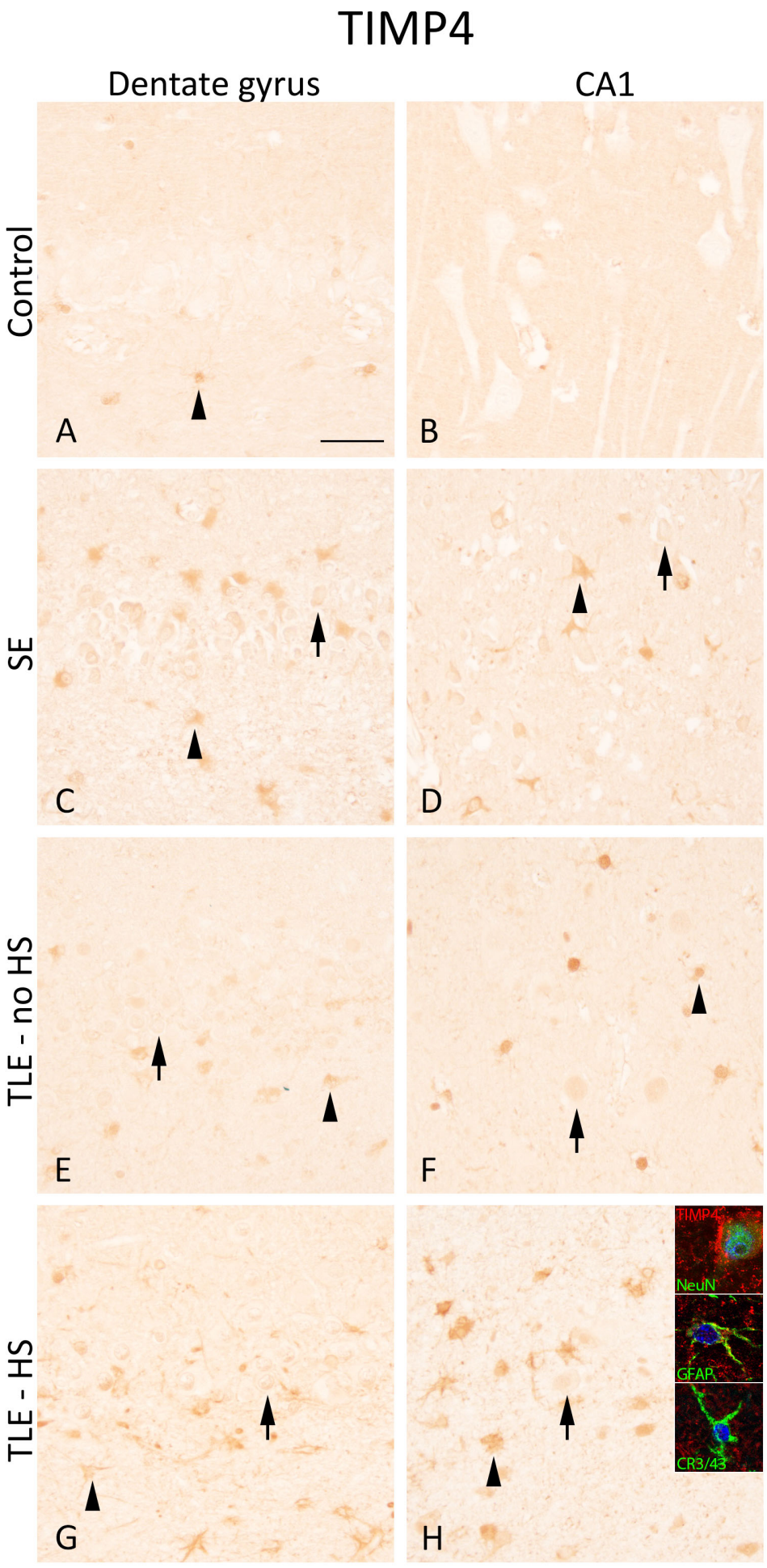


**Supplementary Figure 7. Expression of TIMP4 in the dentate gyrus and CA1 of the human hippocampus**.

In controls, weak expression of TIMP4 was observed in neurons and glia (A, B). In patients who died after a status epilepticus (SE), higher expression of TIMP4 is seen in both neurons and glia (C, D). The same accounts for temporal lobe epilepsy (TLE) patients; both neurons and glia show higher expression of TIMP4 (E-H). HS, hippocampal sclerosis. Scale bar= 50 µm. Arrowheads indicate positive cells with glial morphology, arrows indicate positive neurons. Insets depict double labeling of TIMP4 in NeuN-positive cells (neurons) and GFAP-positive cells (astrocytes), but not in CR3/43-positive cells (microglia).

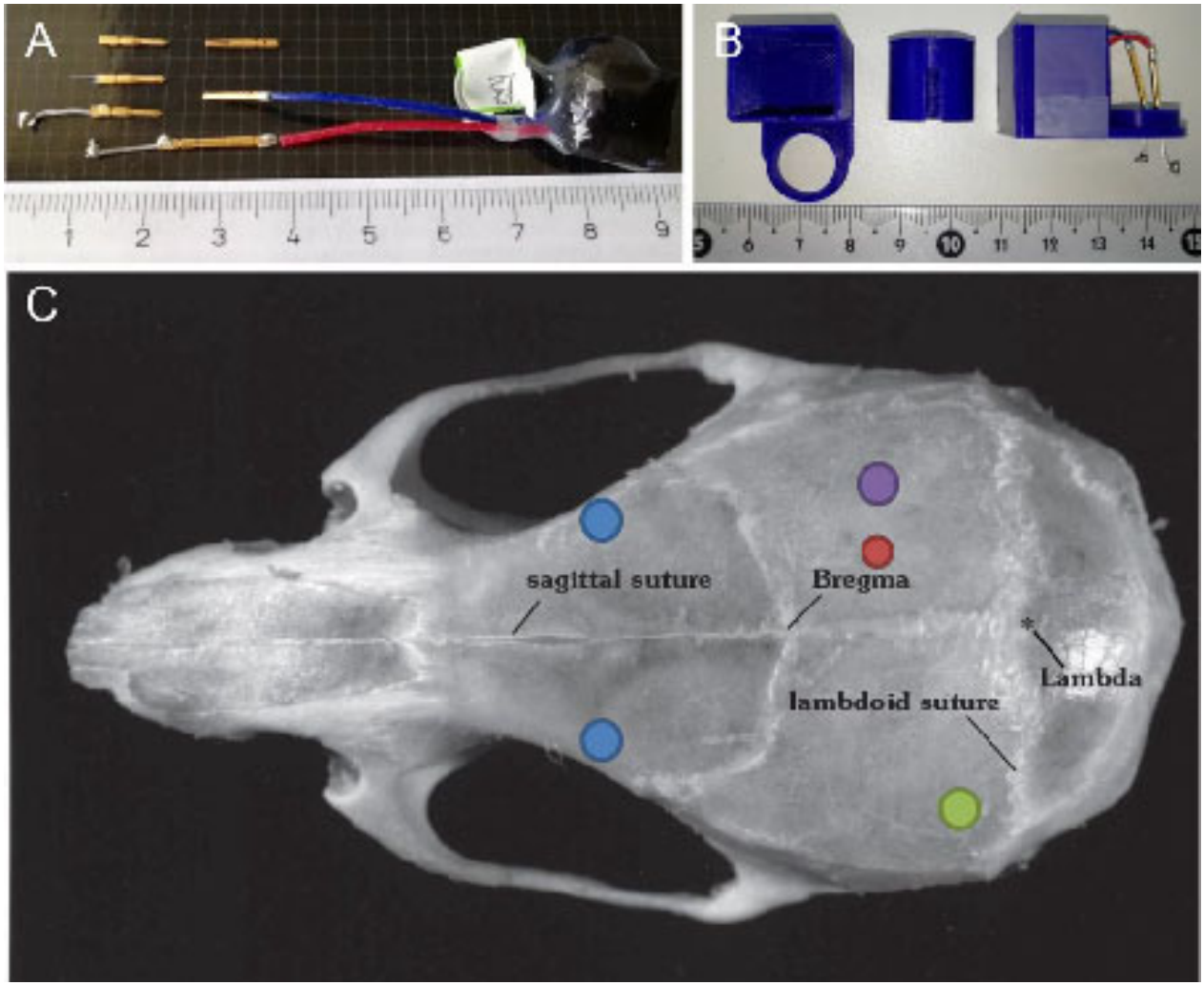


**Supplementary Figure 8. Components of the telemetric EEG recording system.** (A) The A-3028 neurotransmitter (Open Source Instruments, USA) was soldered to a female pin connector (cat: 520100, Science Products, Germany); skull electrode (mouse screw with 10 mm wire, cat: E363/96/1.6/Spc, Bilaney Consultants GmbH) was soldered to a male pin connector (cat: 520200, Science Products, Germany). Alternatively, intracranial electrodes could be made by soldering Teflon coated tungsten wire (cat: WT-2T; coated diameter: 102 µm; bare wire diameter: 50 µm; Science Products, Germany) onto the male pin connector mentioned above. (B) Image of 3D-printed headstage. The body part weights 1.9 g, including a chamber for transmitter (18.5 x 16.5 x 20 mm) and an annulus opening area (inner diameter: 12.15 mm; outer diameter: 14.15 mm) for electrodes and cannulas implantation; the cap part (inner diameter: 12.25 mm; outer diameter: 14.25 mm; height: 15 mm) weights 0.9 g, is designed to protect the electrodes and cannulas in the annulus area. Files for printing of necessary components can be obtained upon a written request to Alexander.Dityatev@dzne.de. (C) Coordinates of implantations were selected on the basis of Paxinos stereotaxic atlas for mouse brain (the 3rd edition). Red dot: cannula (AP, -1.94; ML, +2.0); purple dot: active electrode (AP, -1.94; ML, +2.0 mm); green dot: ground electrode (AP, -3.50; ML, -3.5 mm); blue dot: anchor screws (AP, +2.5; ML, ±1.7 mm).

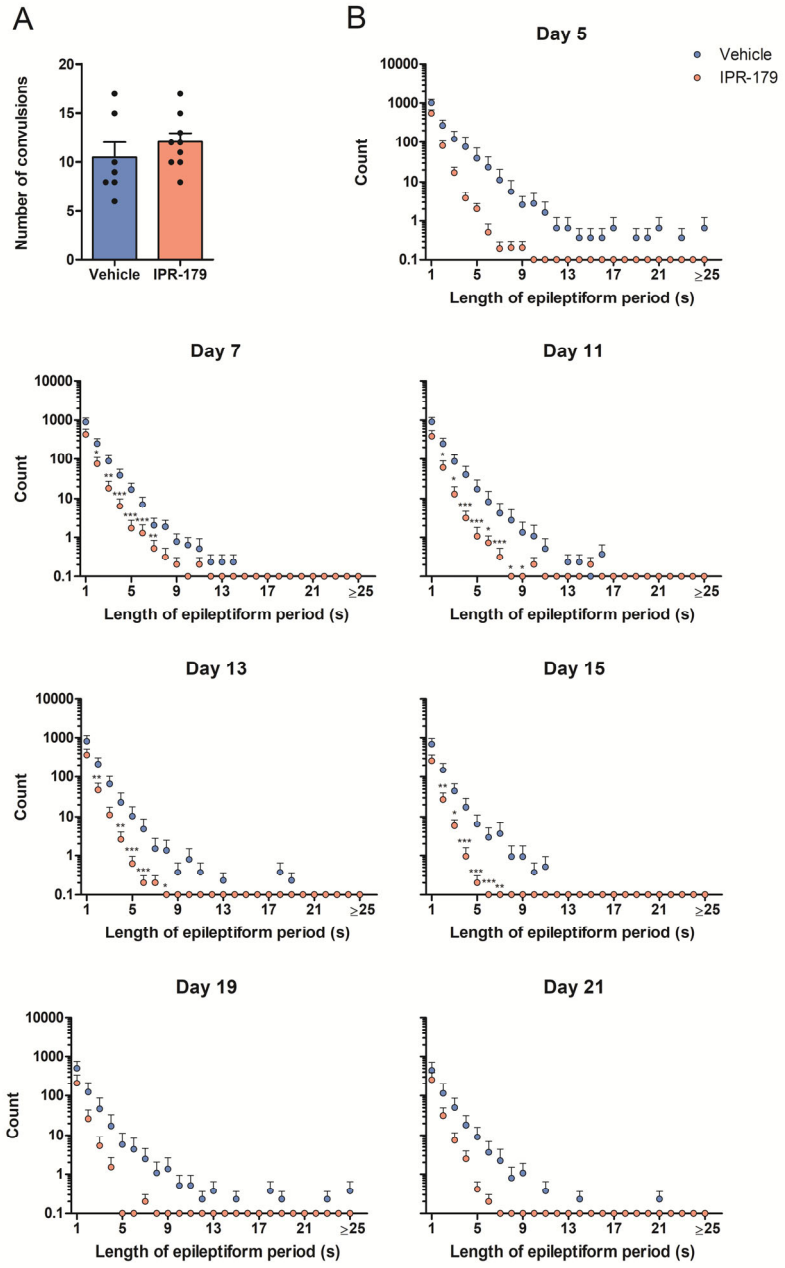


**Supplementary Figure 9. Analysis of convulsions and EEG recordings of animals with long-term IPR-179/vehicle treatment.** (A) The number of convulsions during the first hour after kainic acid injection was not different between groups ($P$ = 0.673, two-sided unpaired t-test). Line and error bars represent means + SEMs. (B) Two-way RM ANOVA revealed a difference in distribution of epileptiform activity on day 5 ($F_{(1, 14)}$ =4.163, $P$=0.061), day 7 ($F_{(1, 14)}$ =4.900, $P$=0.044), day11 ($F_{(1, 14)}$ =5.852, $P$=0.030), day 13 ($F_{(1, 14)}$ =4.591, $P$=0.050), day 15 ($F_{(1, 14)}$ =6.568, $P$=0.023), day 19 ($F_{(1, 14)}$ =3.674, $P$=0.076) and day 21 ($F_{(1, 14)}$ =4.037, $P$=0.064). Data are presented as means + SEMs. In histograms, dots represent the individual samples, while bars indicate group mean + SEM, *, $P$<0.05; **, $P$<0.01; ***, $P$<0.001, Holm-Sidak post-hoc test.

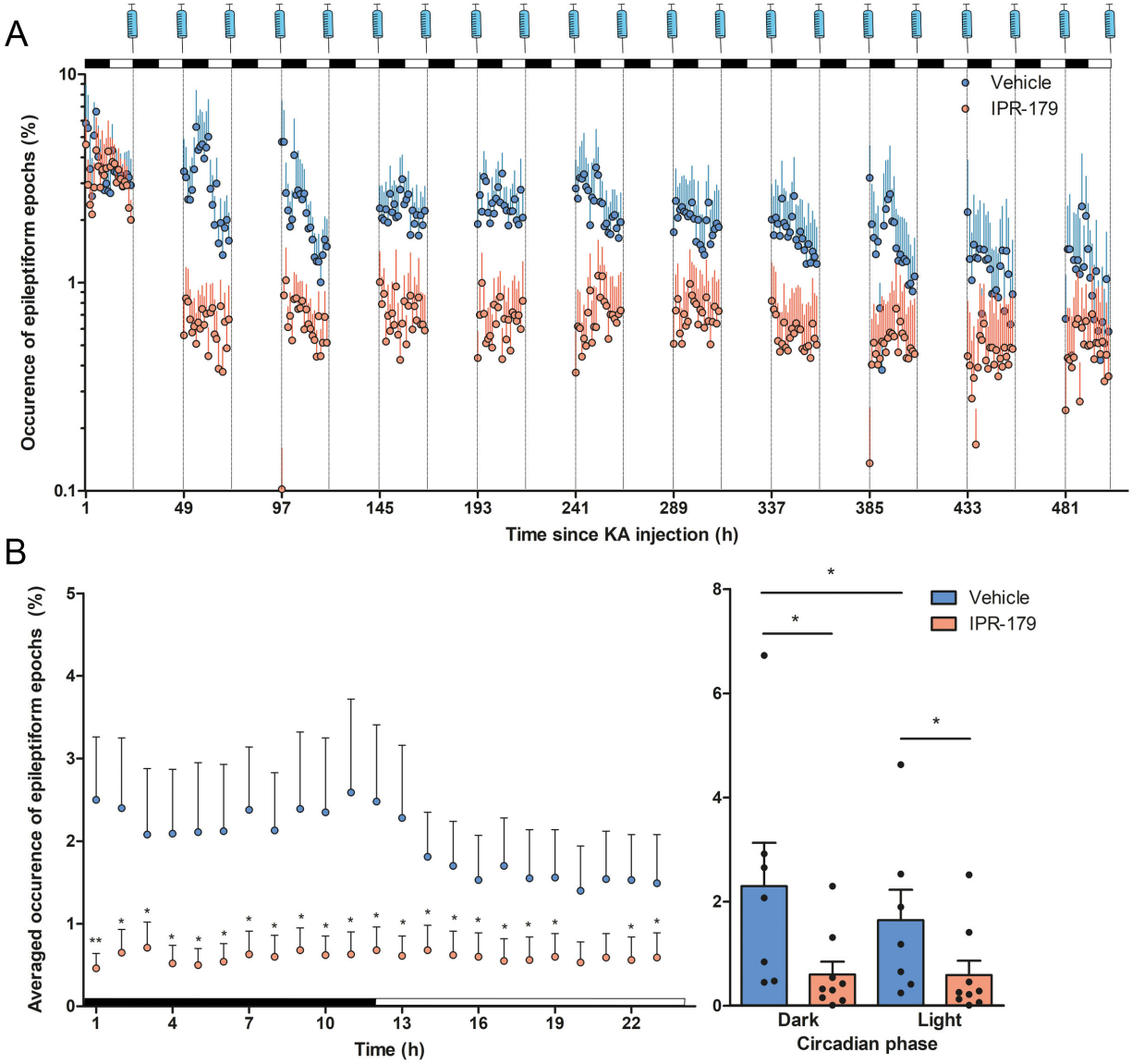


**Supplementary Figure 10. Analysis of epileptiform activity as a function of circadian rhythm of animals with long-term IPR-179/vehicle treatment.** (A) A general overview of epileptiform activity (% of ictal and interictal events) for all recorded days after kainic acid injection. Note that on the first day of recording (before treatment) there is no difference between groups but from day 3 there is a persistent suppression of epileptiform activity by IPR-179. Dark/light cycle and time of IPR-179 administration are shown above the graph. (B) Epileptiform activity as a function of time after daily i.p. injections averaged for days 3-21. Two-way RM ANOVA revealed a significant effect of treatment averaged by the circadian hour ($F_{(1, 14)}$ =6.349, P=0.025) and by the circadian phase (F (1, 14) =5.127, P=0.040). *, P<0.05; **, P<0.01, Holm-Sidak post-hoc test. Data are presented as means + SEMs using Log10 scale in A, dots in histograms represent individual samples.

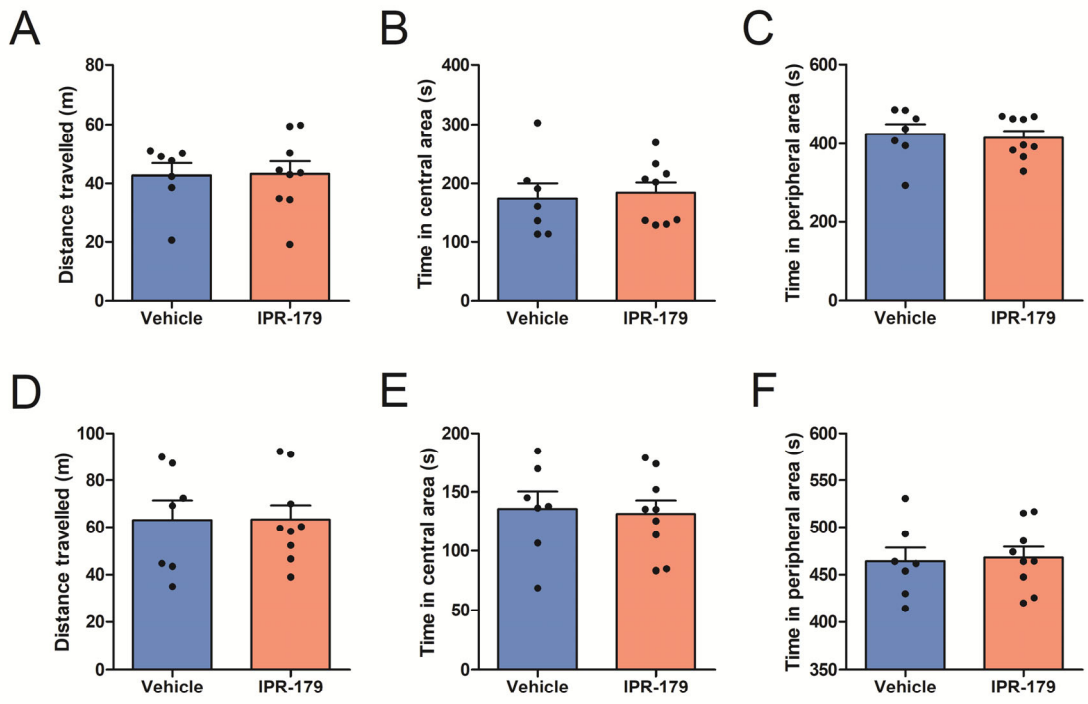


**Supplementary Figure 11. Locomotor activity in the open field of animals with long-term IPR-179/vehicle treatment.** Measurements were done for 10 minutes before (A-C) and three weeks after (D-F) KA injection. In terms of the distance travelled (A, D), time spent in the central area (B, E) and peripheral area (C, F), IPR-179 treated mice were not statistically different from the vehicle-treated mice ($P > 0.05$, two-sided unpaired t-test). Data are presented as means +SEMs, dots in histograms represent individual samples.

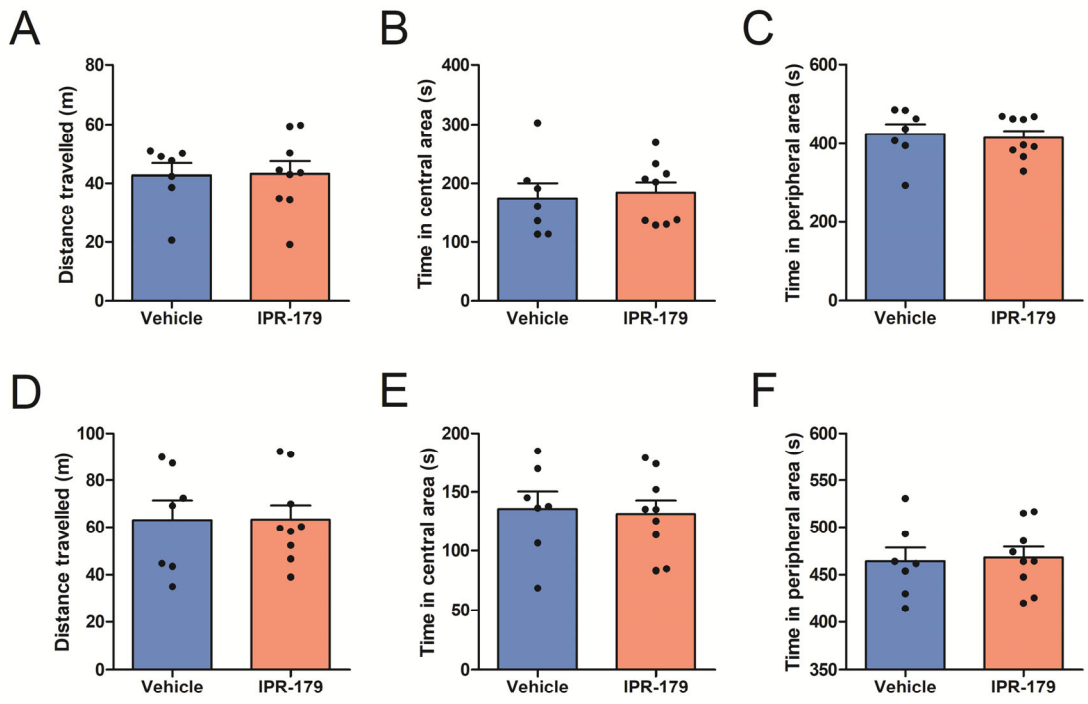


**Supplementary Figure 12. Convulsion and epileptiform epochs numbers on different recording days of animals with short-term IPR-179/vehicle treatment.** After KA injection, animals were randomly allocated into two groups to counterbalance the severity of SE. The convulsion number is shown every 10 minutes (A) as well as the total number for the first hour after KA injection (B). (C) The epileptiform epoch counts before vehicle/IPR-179 treatment: no difference between groups. (D) Typical distribution of epileptiform epoch counts as a function of period length. Two-way RM ANOVA reveals significant differences at day 2 ($F_{(1, 14)}$ =17.619, P=0.0009), day 14 ($F_{(1, 14)}$ =5.437, P=0.0352) and day 48 ($F_{(1, 14)}$ =8.990, P=0.0096). *P<0.05, **P<0.01, ***P<0.001, post-hoc Holm-Sidak test. Data are presented as means +SEMs, dots in histograms represent individual samples.

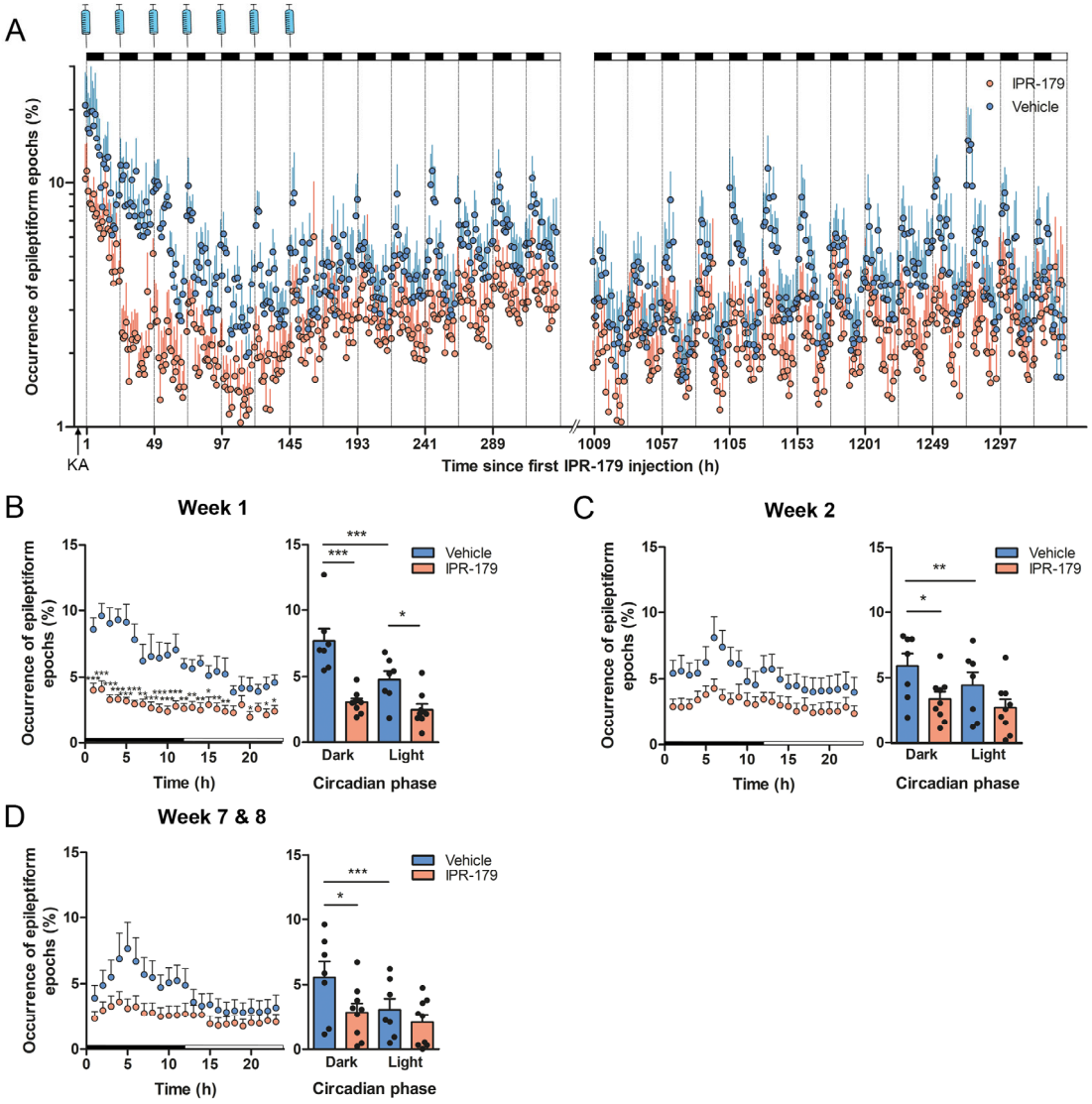


**Supplementary Figure 13. Analysis of epileptiform activity as a function of circadian rhythm of animals with short-term IPR-179/vehicle administration.** (A) A general overview of epileptiform activity (% of ictal and interictal events) for all recorded days after KA injection. Dark/light cycle and time of IPR-179 administration are shown above the graph. Epileptiform activity as a function of time after daily i.p. injections averaged for the week of IPR-179 treatment (week 1; B), the first week after treatment withdrawal (week 2; C) and after long-term treatment withdrawal (weeks 7+8; D). Two-way repeated measures ANOVA reveals a significant effect of IPR-179 on epileptiform epoch distribution as a function of the circadian hour during week 1 ($F_{(22, 308)}$ =10.906, P<0.0001), week 2 ($F_{(22, 308)}$ =6.375, P<0.0001) and weeks 7+8 ($F_{(22, 308)}$ =10.0784, P<0.0001). Two-way repeated measures ANOVA of epileptiform activity during circadian phases reveals a significant effect of treatment during week 1 ($F_{(1, 14)}$=28.33, P=0.0001), week 2 ($F_{(1, 14)}$ =12.39, P=0.0034) and weeks 7 & 8 ($F_{(1, 14)}$ =26.72, P=0.0001). $^{+}$, P<0.1, *, P<0.05; **, P<0.01; ***, P<0.001, post-hoc Holm-Sidak test. Data are presented as means + SEM using Log10 scale in A, dots in histograms represent individual samples.

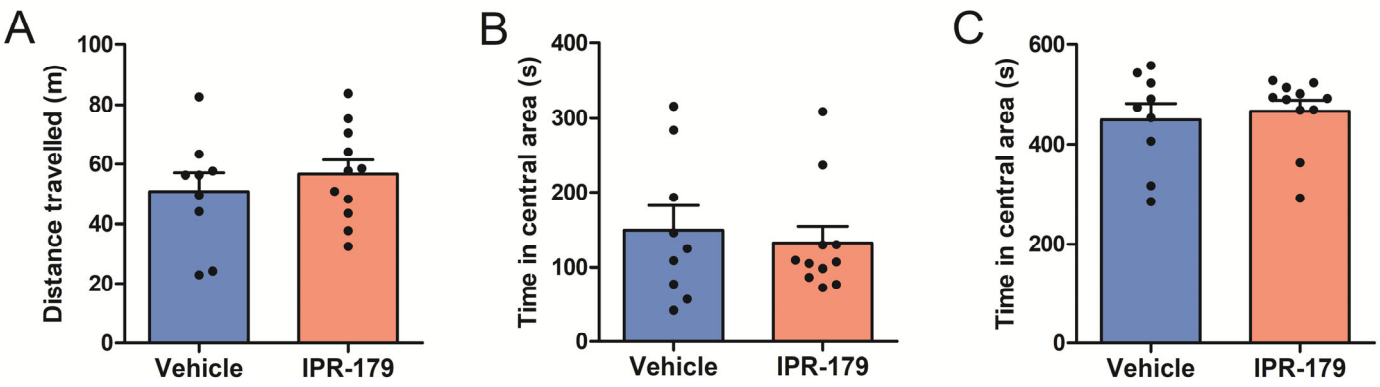


**Supplementary Figure 14. Locomotor activity in the open field of animals with short-term IPR-179/vehicle treatment.** Measurements were done for 10 minutes four weeks after KA injection. In terms of the distance traveled (A), time spent in the central area (B) and the peripheral area (C), IPR-179 treated mice were not statistically different from the vehicle-treated mice ($P > 0.05$, two-sided unpaired t-test). Data are presented as means +SEMs, dots in histograms represent individual samples.

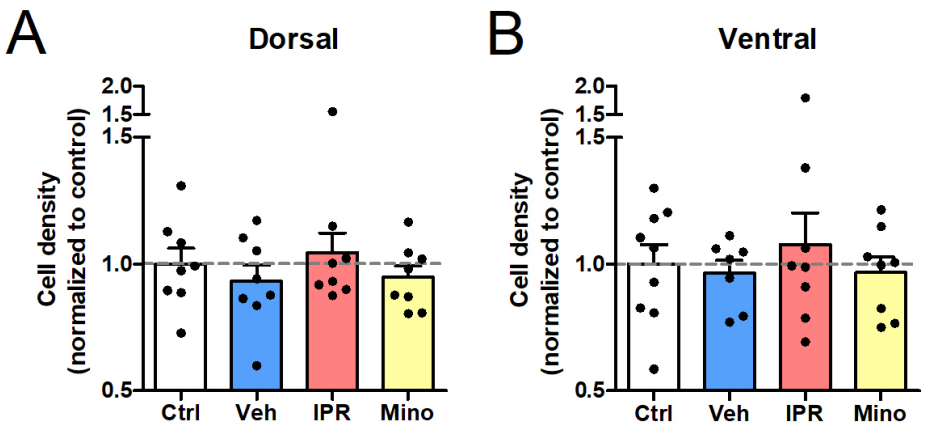


**Supplementary figure 15. Neuronal density in the hippocampus.** Neurons, identified by NeuN immunohistochemistry, were counted in the hilus of the dorsal and ventral hippocampus. A trend towards a lower neuronal density in the hilus of both the dorsal (A) and ventral (B) hippocampus was observed in kindled, vehicle (Veh)-treated rats as compared to control (Ctrl) rats. In contrast, a trend towards a higher neuronal density was observed in IPR-179-treated rats compared to vehicle-treated animals, while this was absent in minocycline (Mino)-treated rats. Data are presented as means +SEMs, dots in histograms represent individual samples.

## Supplementary Tables

**Supplementary Table 1. The inhibitory potency of IPR-179, showing its selectivity for MMP2 and MMP9.**

| | $IC_{50}$ (nM) |
|---|---|
| **MMP2** | 656 ± 9 |
| **MMP9** | 310 ± 5 |
| **MMP1** | > 10,000 |
| **MMP3** | > 10,000 |
| **MMP7** | > 10,000 |
| **MMP8** | > 3352 ± 385 |
| **ADAM10** | 48,900 ± 3634 |
| **ADAM17** | 16,400 ± 1676 |
| **Prolyl oligopeptidase** | > 200,000 |
| **Dipeptidyl peptidase IV** | > 200,000 |

**Supplementary Table 2. Immunoreactivity scores of MMP2, MMP3, MMP9 and MMP14 protein in dentate gyrus and CA1 of human hippocampus**

| | | Dentate gyrus | | CA1 | |
|---|---|---|---|---|---|
| | | **neurons** | **glia** | **neurons** | **glia** |
| **MMP2** | **Control** | 6 (3-6) | 0 (0-2) | 9 (3-9) | 0 (0-4) |
| | **SE** | 12 (9-12)* | 9 (4-9)* | 12 (9-12)* | 9 (6-9)** |
| | **TLE - no HS** | 6 (3-9) | 0 (0-1)^ | 9 (3-12) | 4 (3-12)* |
| | **TLE - HS** | 9 (6-12)* | 7.5 (0-9)* | 10.5 (6-12) | 12 (4-12)** |
| **MMP3** | **Control** | 1 | 3 (3-6) | 1 | 3 (2-3) |
| | **SE** | 1 (1-6) | 9 (9-12)** | 6 (3-6)* | 12** |
| | **TLE - no HS** | 1 (1-6) | 8 (3-12)* | 1 (1-6)^ | 8 (3-8)*^^^ |
| | **TLE - HS** | 1 (1-9) | 12 (4-12)** | 6 (6-9)*** | 12 (9-12)*** |
| **MMP9** | **Control** | 3 (3-6) | 0 | 3 (3-6) | 0 (0-1) |
| | **SE** | 9 (6-12)* | 12 (1-12)** | 9 (6-12)* | 9 (1-12)* |
| | **TLE - no HS** | 9 (6-9)* | 4 (1-9)** | 9 (9-12)** | 1 (1-9)* |
| | **TLE - HS** | 9 (6-12)** | 7.5 (2-12)** | 10.5 (9-12)*** | 9 (4-12)** |
| **MMP14** | **Control** | 9 (6-9) | 1.5 (0-4) | 9 (3-9) | 4 (0-4) |
| | **SE** | 12 (9-12)** | 6 (3-9)** | 9 (9-12)** | 6 (4-9)** |
| | **TLE - no HS** | 7.5 (6-9) | 5 (4-6) | 9 (6-9) | 5 (3-12)* |
| | **TLE - HS** | 12 (9-12) | 10.5 (4-12)** | 9 (6-12)* | 9 (4-12)*** |

The immunoreactivity score (IRS) of MMP2, MMP3, MMP9, and MMP14 is given as median (minimum-maximum) and defined as intensity score (1: no; 2: weak; 3: moderate; 4: strong IR) multiplied by frequency score (0: no; 1: single to 10%; 2: 11-50%; 3: >50%). Different compared to control, $P<0.05$: *, $P<0.01$: ** $P<0.001$: ***. Different compared to HS, $P<0.05$: ^, $P<0.01$: ^^, $P<0.001$: ^^^. SE, status epilepticus; TLE, temporal lobe epilepsy, HS; hippocampal sclerosis.

**Supplementary Table 3. Immunoreactivity scores of TIMP1, TIMP2, TIMP3 and TIMP4 protein in dentate gyrus and CA1 of human hippocampus**

| | | Dentate gyrus | | CA1 | |
|---|---|---|---|---|---|
| | | **neurons** | **glia** | **neurons** | **glia** |
| **TIMP1** | **Control** | 3 (3-9) | 3 (0-9) | 3 (3-6) | 3 (0-8) |
| | **SE** | 6 (3-8) | 9 (4-12)* | 4 (3-6) | 9 (9-12)** |
| | **TLE - no HS** | 3 (3-6) | 4 (2-9)^ | 3 (3-9)^ | 3 (1-9)^ |
| | **TLE - HS** | 6 (3-8) | 9 (6-9)** | 10.5 (3-12)* | 9 (2-12)*^ |
| **TIMP2** | **Control** | 6 (3-6) | 2 (1-4) | 6 (3-9) | 1 (1-3) |
| | **SE** | 9 (6-12)* | 9 (4-9)** | 9 (6-12) | 9 (4-9)** |
| | **TLE - no HS** | 9 (6-9)* | 5 (2-12) | 9 (6-9)^ | 6 (2-9)*^ |
| | **TLE - HS** | 7.5 (3-12) | 9 (2-12)* | 10.5 (9-12)** | 9 (4-12)** |
| **TIMP3** | **Control** | 3 (3-9) | 0 | 6 (3-9) | 0 |
| | **SE** | 3 (3-6) | 3 (0-3)* | 6 (3-9) | 1 (0-3) |
| | **TLE - no HS** | 12 (9-12)** | 9 (4-9)** | 12** | 9 (6-9)** |
| | **TLE - HS** | 12*** | 9*** | 12*** | 9 (9-12)*** |
| **TIMP4** | **Control** | 3 | 4 (3-8) | 3 | 4 (4-8) |
| | **SE** | 6 (3-6)* | 12 (6-12)* | 6 (3-6) | 12 (8-12)** |
| | **TLE - no HS** | 6 (3-6)* | 9 (9-12)** | 6 (3-6)* | 9 (6-12)*^^ |
| | **TLE - HS** | 6 (3-9)* | 12 (3-12)** | 6 (3-9)* | 12*** |

The immunoreactivity score (IRS) of TIMP1, TIMP2, TIMP3, and TIMP4 is given as median (minimum-maximum) and defined as intensity score (1: no; 2: weak; 3: moderate; 4: strong IR) multiplied by frequency score (0: no; 1: single to 10%; 2: 11-50%; 3: >50%). Different compared to control, $P<0.05$: *, $P<0.01$: ** $P<0.001$: ***. Different compared to HS, $P<0.05$: ^, $P<0.01$: ^^, $P<0.001$: ^^^. SE, status epilepticus; TLE, temporal lobe epilepsy, HS; hippocampal sclerosis.

**Supplementary Table 4. Immunoreactivity score of MMP9 protein in dentate gyrus and CA1 of post-SE rat hippocampus**

| | Dentate gyrus | | CA1 | |
|---|---|---|---|---|
| | **neurons** | **glia** | **neurons** | **glia** |
| **Control** | 3 (3-6) | 0 (0-1) | 3 (3-9) | 0 |
| **Acute** | 9 (3-9) | 0 (0-6) | 9 (3-9) | 2 (0-6)* |
| **Latent** | 9 (6-9)* | 4 (0-6)* | 9 (6-9) | 1.5 (0-6)* |
| **Chronic p** | 9** | 1.5 (0-6) | 10.5 (9-12)** | 0 (0-6) |
| **Chronic np** | 9 (6-9)* | 0 (0-6) | 12 (6-12)* | 0 (0-6) |

The immunoreactivity score is given as median (minimum-maximum) and defined as intensity score (1: no; 2: weak; 3: moderate; 4: strong IR) multiplied by frequency score (0: no; 1: single to 10%; 2: 11-50%; 3: >50%). Different compared to control, $P<0.05$: *, $P<0.01$: **. P, progressive; np, non-progressive.

**Supplementary Table 5. Clinical features of patients used for IHC and RT-qPCR analysis.**

| Case number | | Pathology | Gender | Age | Duration of epilepsy (years) | Age at onset | Number of seizures (per month) | Cause of death |
|---|---|---|---|---|---|---|---|---|
| 1 | a | Control | f | 64 | N.A. | N.A. | N.A. | myocard infarction |
| 2 | a, b | Control | m | 31 | N.A. | N.A. | N.A. | myocard infarction |
| 3 | a | Control | f | 46 | N.A. | N.A. | N.A. | oesofagus carcinoma |
| 4 | a | Control | f | 25 | N.A. | N.A. | N.A. | hyperkalemia |
| 5 | a | Control | f | 39 | N.A. | N.A. | N.A. | status asthmaticus with acute heart failure |
| 6 | a, b | Control | m | 49 | N.A. | N.A. | N.A. | myocarditis and pneumonia |
| 7 | a | Control | f | 39 | N.A. | N.A. | N.A. | cervix tumor |
| 8 | a | Control | m | 48 | N.A. | N.A. | N.A. | myocard infarction |
| 9 | b | Control | m | 75 | N.A. | N.A. | N.A. | pneumonia |
| 10 | b | Control | f | 35 | N.A. | N.A. | N.A. | complications with lepra |
| 11 | b | Control | m | 69 | N.A. | N.A. | N.A. | adenocarcinoma |
| 12 | b | Control | m | 79 | N.A. | N.A. | N.A. | liver failure with portal thrombosis |
| 13 | b | Control | m | 72 | N.A. | N.A. | N.A. | oropharynxcarcinoma |
| 14 | b | Control | f | 81 | N.A. | N.A. | N.A. | peritonitis after diverticulitis |
| 15 | b | Control | f | 68 | N.A. | N.A. | N.A. | hemorragische pneumonia |
| 16 | b | Control | m | 86 | N.A. | N.A. | N.A. | pneumonia |
| 17 | b | Control | f | 71 | N.A. | N.A. | N.A. | post-operative complications after mitral valve replacement |
| 18 | b | Control | m | 60 | N.A. | N.A. | N.A. | pneumonia |
| 19 | a | SE | f | 64 | N.A. | N.A. | N.A. | sepsis |
| 20 | a | SE | f | 54 | N.A. | N.A. | N.A. | sepsis |
| 21 | a | SE | f | 79 | N.A. | N.A. | N.A. | respiratory insufficiency |
| 22 | a | SE | m | 67 | N.A. | N.A. | N.A. | sepsis |
| 23 | a | SE | f | 87 | N.A. | N.A. | N.A. | aneurysm |
| 24 | a, b | TLE - HS | f | 31 | 10 | 21 | 4 | N.A. |
| 25 | a, b | TLE - HS | m | 49 | 41 | 8 | 2 | N.A. |
| 26 | a, b | TLE - HS | m | 38 | 8 | 30 | 6 | N.A. |
| 27 | a, b | TLE - HS | f | 44 | 22 | 22 | 3 | N.A. |

| | | | | | | | | |
|---|---|---|---|---|---|---|---|---|
| 28 | a, b | TLE - HS | m | 43 | 40 | 3 | 8 | N.A. |
| 29 | a | TLE - HS | m | 29 | 11 | 18 | 32 | N.A. |
| 30 | a | TLE - HS | f | 29 | 16 | 13 | 32.17 | N.A. |
| 31 | a | TLE - HS | m | 24 | 16 | 8 | 1.5 | N.A. |
| 32 | a | TLE - HS | m | 25 | 19 | 6 | 5 | N.A. |
| 33 | a | TLE - HS | m | 39 | 5 | 34 | 32 | N.A. |
| 34 | b | TLE - HS | f | 57 | 11 | 46 | 1 | N.A. |
| 35 | b | TLE - HS | m | 40 | 23 | 17 | 4.5 | N.A. |
| 36 | b | TLE - HS | f | 11 | 1 | 10 | 5 | N.A. |
| 37 | b | TLE - HS | f | 41 | 11 | 30 | 5 | N.A. |
| 38 | b | TLE - HS | f | 47 | 38 | 9 | 10 | N.A. |
| 39 | b | TLE - HS | f | 34 | 31 | 3 | 3 | N.A. |
| 40 | b | TLE - HS | f | 20 | 15 | 5 | 16 | N.A. |
| 41 | b | TLE - HS | m | 14 | 13 | 1 | 2.5 | N.A. |
| 42 | b | TLE - HS | m | 8 | 2 | 6 | 150 | N.A. |
| 43 | a | TLE - noHS | m | 51 | 2 | 49 | 4 | N.A. |
| 44 | a | TLE - noHS | m | 45 | 27 | 18 | 2 | N.A. |
| 45 | a | TLE - noHS | m | 41 | 33 | 8 | 16 | N.A. |
| 46 | a | TLE - noHS | m | 24 | 9 | 15 | 8 | N.A. |
| 47 | a | TLE - noHS | f | 35 | 3 | 32 | 13 | N.A. |

a, immunohistochemistry; b, real-time quantitative polymerase chain reaction; f, female; m, male; SE, status epilepticus; TLE, temporal lobe epilepsy; HS, hippocampal
sclerosis; no – HS, without hippocampal sclerosis; N.A. not applicable.

**Supplementary Table 6. Primer sequences used for quantitative RT-qPCR analysis using human brain. tissue**

| Gene | Primer | Sequence |
|---|---|---|
| ***MMP2*** | Forward | ATAACCTGGATGCCGTCGT |
| | Reverse | AGGCACCCTTGAAGAAGTAGC |
| ***MMP3*** | Forward | CTCCAACCGTGAGGAAAATC |
| | Reverse | CATGGAATTTCTCTTCTCATCAAA |
| ***MMP9*** | Forward | GAACCAATCTCACCGACAGG |
| | Reverse | GCCACCCGAGTGTAACCATA |
| ***MMP14*** | Forward | GCCTTGGACTGTCAGGAATG |
| | Reverse | AGGGGTCACTGGAATGCTC |
| ***TIMP1*** | Forward | GGGCTTCACCAAGACCTACA |
| | Reverse | TGCAGGGGATGGATAAACAG |
| ***TIMP2*** | Forward | TGCAGATGTAGTGATCAGGGC |
| | Reverse | TCTCAGGCCCTTTGAACATC |
| ***TIMP3*** | Forward | GCTGGAGGTCAACAAGTACCA |
| | Reverse | CACAGCCCCGTGTACATCT |
| ***TIMP4*** | Forward | TTGGTGCAGAGGGAAAGTCT |
| | Reverse | GGTACTGTGTAGCAGGTGGTGA |
| ***EF1α*** | Forward | ATCCACCTTTGGGTCGCTTT |
| | Reverse | CCGCAACTGTCTGTCTCATATCAC |
| ***C1orf43*** | Forward | GATTTCCCTGGGTTTCCAGT |
| | Reverse | ATTCGACTCTCCAGGGTTCA |

**Supplementary Table 7. Primer sequences used for quantitative RT-qPCR analysis using rat brain. tissue**

| Gene | Primer | Sequence |
|---|---|---|
| ***Mmp2*** | Forward | CACCACCGAGGATTATGACC |
| | Reverse | CACCCACAGTGGACATAGCA |
| ***Mmp3*** | Forward | TTGTCCTTCGATGCAGTCAG |
| | Reverse | GGGGTCCTGAGAGATTTTCG |
| ***Mmp9*** | Forward | AAGCTGTATGGCTTCTGTCC |
| | Reverse | GAAACCCCACTTCTTGTCAG |
| ***Mmp14*** | Forward | AACTTCGTGTTGCCTGATGA |
| | Reverse | TTTGTGGGTGACCCTGACTT |
| ***Gapdh*** | Forward | ATGACTCTACCCACGGCAAG |
| | Reverse | TACTCAGCACCAGCATCACC |
| **Cyclophilin A** | Forward | CCCACCGTGTTCTTCGACAT |
| | Reverse | AAACAGCTCGAAGCAGACGC |

## Supplementary Table 8. Statistical analysis of behavioral data.

| Figure | Measure | Group/ Variable 1 | Group/ Variable 2 | Data from the same subject | Normality test (Shapiro-Wilk) | Comparison test applied (as suggested by Sigmaplot) | P-value reported in the Figure | Non-parametric test | P-value |
|---|---|---|---|---|---|---|---|---|---|
| **7B(left), blue** | NORT, exploration time, in animals before long-term vehicle treatment | Familiar object | Novel object | Yes | $P = 0.082$ | Two-tailed paired t-test | 0.046 | Wilcoxon signed rank test | 0.016 |
| **7B(left), red** | NORT, exploration time, in animals before long-term IPR-179 treatment | Familiar object | Novel object | Yes | $P = 0.060$ | Two-tailed paired t-test | 0.0103 | Wilcoxon signed rank test | 0.0039 |
| **7B(right)** | NORT, discrimination ratio, in animals before long-term treatment | Vehicle group | IPR-179 group | No | $P = 0.208$ | Two-tailed unpaired t-test | 0.834 | Mann-Whitney rank sum test | 1.000 |
| **7C(left), blue** | NORT, exploration time, in animals after long-term vehicle treatment | Familiar object | Novel object | Yes | $P = 0.104$ | Two-tailed paired t-test | 0.784 | Wilcoxon signed rank test | 0.688 |
| **7C(left), red** | NORT, exploration time, in animals after long-term IPR-179 treatment | Familiar object | Novel object | Yes | $P < 0.05$ | Wilcoxon signed rank test | 0.0078 | Wilcoxon signed rank test | 0.0078 |
| **7C(right)** | NORT, discrimination ratio, in animals after long-term treatment | Vehicle group | IPR-179 group | No | $P = 0.591$ | Two-tailed unpaired t-test | 0.044 | Mann-Whitney rank sum test | 0.072 |
| **8F(left), blue** | NORT, exploration time, in animals after short-term vehicle treatment | Familiar object | Novel object | Yes | $P = 0.773$ | Two-tailed paired t-test | 0.587 | Wilcoxon signed rank test | 0.496 |
| **8F(left), red** | NORT, exploration time, in animals after short-term IPR-179 treatment | Familiar object | Novel object | Yes | $P = 0.346$ | Two-tailed paired t-test | 0.0021 | Wilcoxon signed rank test | 0.0068 |
| **8F(right)** | NORT, discrimination ratio, in animals after short-term treatment | Vehicle group | IPR-179 group | No | $P = 0.533$ | Two-tailed unpaired t-test | 0.0031 | Mann-Whitney rank sum test | 0.0049 |
| **8G(left), blue** | NOLT, exploration time, in animals after short-term vehicle treatment | Familiar object | Novel object | Yes | $P = 0.252$ | Two-tailed paired t-test | 0.961 | Wilcoxon signed rank test | 0.734 |
| **8G(left), red** | NOLT, exploration time, in animals after short-term IPR-179 treatment | Familiar object | Novel object | Yes | $P = 0.120$ | Two-tailed paired t-test | 0.0489 | Wilcoxon signed rank test | 0.0645 |
| **8G(right)** | NOLT, discrimination ratio, in animals after short-term treatment | Vehicle group | IPR-179 group | No | $P = 0.651$ | Two-tailed unpaired t-test | 0.0499 | Mann-Whitney rank sum test | 0.0455 |
| **Suppl.11A** | OF, distance travelled, in animals before long-term treatment | Vehicle group | IPR-179 group | No | $P = 0.207$ | Two-tailed unpaired t-test | 0.938 | Mann-Whitney rank sum test | 1.000 |
| **Suppl.11B** | OF, time in central area, in animals before long-term treatment | Vehicle group | IPR-179 group | No | $P = 0.072$ | Two-tailed unpaired t-test | 0.744 | Mann-Whitney rank sum Test | 0.459 |
| **Suppl.11C** | OF, time in peripheral area, in animals before long-term treatment | Vehicle group | IPR-179 group | No | $P = 0.066$ | Two-tailed unpaired t-test | 0.757 | Mann-Whitney rank sum Test | 0.458 |
| **Suppl.11D** | OF, distance travelled, in animals after long-term treatment | Vehicle group | IPR-179 group | No | $P = 0.198$ | Two-tailed unpaired t-test | 0.991 | Mann-Whitney rank sum test | 0.832 |
| **Suppl.11E** | OF, time in central area, in animals after long-term treatment | Vehicle group | IPR-179 group | No | $P = 0.520$ | Two-tailed unpaired t-test | 0.822 | Mann-Whitney rank sum test | 0.672 |
| **Suppl.11F** | OF, time in peripheral area, in animals after long-term treatment | Vehicle group | IPR-179 group | No | $P = 0.531$ | Two-tailed unpaired t-test | 0.820 | Mann-Whitney rank sum test | 0.751 |
| **Suppl.14A** | OF, distance travelled, in animals after short-term treatment | Vehicle group | IPR-179 group | No | $P = 0.827$ | Two-tailed unpaired t-test | 0.462 | Mann-Whitney rank sum test | 0.447 |
| **Suppl.14B** | OF, time in central area, in animals after short-term treatment | Vehicle group | IPR-179 group | No | $P < 0.05$ | Mann-Whitney rank sum test | 0.761 | Mann-Whitney rank Sum test | 0.761 |
| **Suppl.14C** | OF, time in peripheral area, in animals after short-term treatment | Vehicle group | IPR-179 group | No | $P < 0.05$ | Mann-Whitney rank sum test | 0.761 | Mann-Whitney rank sum test | 0.761 |

The P-values obtained by two methods are quite similar in most cases. Two rows in red highlight cases when a non-parametric test shows a tendency, while the t-test indicated a significant difference. OF, open field; NORT, novel object recognition test; NOLT, novel object location test.

## Supplementary References


1. J. A. Gorter, E. A. van Vliet, E. Aronica, F. H. Lopes da Silva, Long-lasting increased excitability differs in dentate gyrus vs. CA1 in freely moving chronic epileptic rats after electrically induced status epilepticus. *Hippocampus* 2002;12(3):311-324.
2. R. J. Racine, Modification of seizure activity by electrical stimulation. II. Motor seizure. *Electroencephalogr Clin Neurophysiol* 1972;32(3):281-294.
3. P. Chang, K. S. Hashemi, M. C. Walker, A novel telemetry system for recording EEG in small animals. *J Neurosci Methods* 2011;201(1):106-115.
4. R. C. Wykes, et al., Optogenetic and potassium channel gene therapy in a rodent model of focal neocortical epilepsy. *Sci Transl Med* 2012;4(161):161ra152.
5. S. Wright, et al., Epileptogenic effects of NMDAR antibodies in a passive transfer mouse model. *Brain* 2015;138(Pt11):3159-3167.
6. M. Leger, et al., Object recognition test in mice. *Nat Protoc* 2013;8(12):2531-2537.
7. G. R. Barker, F. Bird, V. Alexander, E. C. Warburton, Recognition memory for objects, place, and temporal order: a disconnection analysis of the role of the medial prefrontal cortex and perirhinal cortex. *J. Neurosci* 2007;27(11):2948-2957.
8. J. M. Ruijter, et al., Amplification efficiency: linking baseline and bias in the analysis of quantitative PCR data. *Nucleic Acids Res* 2009;37(6):e45.
9. F. Bassil, et al., Region-Specific Alterations of Matrix Metalloproteinase Activity in Multiple System Atrophy. *Mov Disord* 2015;30(13):1802-1812.
10. L. Emdad, et al., Astrocyte elevated gene-1: a novel target for human glioma therapy. *Mol Cancer Ther* 2010;9(1):79-88.
11. P. Grammas, D. Tripathy, A. Sanchez, X. Yin, J. Luo, Brain microvasculature and hypoxia-related proteins in Alzheimer's disease. *Int J Clin Exp Pathol* 2011;4(6):616-627.
12. D. Tripathy, A. Sanchez, X. Yin, J. Luo, J. Martinez, P. Grammas, Thrombin, a mediator of cerebrovascular inflammation in AD and hypoxia. *Front Aging Neurosci* 2013;5:19.
13. A. Lamarca, et al., Uridine 5'-triphosphate promotes in vitro Schwannoma cell migration through matrix metalloproteinase-2 activation. *PloS one* 2014;9(6):e98998.
14. F. Zhao, et al., Cause and Effect Relationship between Changes in Scleral Matrix Metallopeptidase-2 Expression and Myopia Development in Mice. *Am J Pathol* 2018;188(8):1754-1767.
15. I. Van Hove, K. Lemmens, S. Van de Velde, M. Verslegers, L. Moons, Matrix metalloproteinase-3 in the central nervous system: a look on the bright side. *J Neurochem* 2012;123(2):203-216.
16. I. Van Hove, et al., MMP-3 Deficiency Alleviates Endotoxin-Induced Acute Inflammation in the Posterior Eye Segment. *Int J Mol Sci* 2016;17(11):1825.
17. W. Maetzler, et al., GDF15/MIC1 and MMP9 Cerebrospinal Fluid Levels in Parkinson's Disease and Lewy Body Dementia. *PloS one* 2016;11(3):e0149349.
18. E. Pivetta, et al., MMP-13 stimulates osteoclast differentiation and activation in tumour breast bone metastases. *Breast Cancer Res* 2011;13(5):R105.
19. P. Sahay, et al., Functional Activity of Matrix Metalloproteinases 2 and 9 in Tears of Patients With Glaucoma. *Invest Ophthalmol Vis Sci* 2017;58(6):Bio106-bio113.
20. T. Yamada, Y. Yoshiyama, H. Sato, M. Seiki, A. Shinagawa, M. Takahashi, White matter microglia produce membrane-type matrix metalloprotease, an activator of gelatinase A, in human brain tissues. *Acta Neuropathol* 1995;90(5):421-424.

21. M. Kajita, et al., Membrane-type 1 matrix metalloproteinase cleaves CD44 and promotes cell migration. *J Cell Bio* 2001;153(5):893-904.
22. P. A. Klenotic, et al., Histidine-rich glycoprotein modulates the anti-angiogenic effects of vasculostatin. *Am J Pathol* 2010;176(4):2039-2050.
23. D. W. M. Broekaart, et al., Increased expression of (immuno)proteasome subunits during epileptogenesis is attenuated by inhibition of the mammalian target of rapamycin pathway. *Epilepsia* 2017;58(8):1462-1472.
24. J. Vandooren, et al., Gelatin degradation assay reveals MMP-9 inhibitors and function of O-glycosylated domain. *World J Biol Chem* 2011;2(1):14-24.
25. T. Tarragó, S. Frutos, R. A. Rodriguez-Mias, E. Giralt, Identification by 19F NMR of traditional Chinese medicinal plants possessing prolyl oligopeptidase inhibitory activity. *Chembiochem* 2006;7(5):827-833.
26. K. Toide, Y. Iwamoto, T. Fujiwara, H. Abe, JTP-4819: a novel prolyl endopeptidase inhibitor with potential as a cognitive enhancer. *J Pharmacol Exp Ther* 1995;274(3):1370-1378.
27. F. Checler, J. P. Vincent, P. Kitabgi, Inactivation of neurotensin by rat brain synaptic membranes partly occurs through cleavage at the Arg8-Arg9 peptide bond by a metalloendopeptidase. *J Neurochem* 1985;45(5):1509-1513.